Numerical integration of variational equations

Ch. Skokos[1] and E. Gerlach[2]
[1]*Max Planck Institute for the Physics of Complex Systems, Nöthnitzer Str. 38, D-01187 Dresden, Germany*
[2]*Lohrmann Observatory, Technical University Dresden, D-01062 Dresden, Germany*
(Received 1 June 2010; published 30 September 2010)

We present and compare different numerical schemes for the integration of the variational equations of autonomous Hamiltonian systems whose kinetic energy is quadratic in the generalized momenta and whose potential is a function of the generalized positions. We apply these techniques to Hamiltonian systems of various degrees of freedom and investigate their efficiency in accurately reproducing well-known properties of chaos indicators such as the Lyapunov characteristic exponents and the generalized alignment indices. We find that the best numerical performance is exhibited by the "tangent map method," a scheme based on symplectic integration techniques which proves to be optimal in speed and accuracy. According to this method, a symplectic integrator is used to approximate the solution of the Hamilton equations of motion by the repeated action of a symplectic map S, while the corresponding tangent map TS is used for the integration of the variational equations. A simple and systematic technique to construct TS is also presented.

DOI: 10.1103/PhysRevE.82.036704 PACS number(s): 45.10.−b, 05.45.−a, 02.60.Cb

I. INTRODUCTION

Numerical integration is very often the only available tool for investigating the properties of nonlinear dynamical systems. Different numerical techniques [1,2] have been developed over the years which permit the fast and accurate time evolution of orbits in such systems.

Of particular interest are the so-called *symplectic integrators* which are numerical methods specifically aimed at advancing in time the solution of Hamiltonian systems with the aid of symplectic maps (see, for example, Chap. VI of [2], [3] and references therein). Another challenging numerical task in conservative Hamiltonian systems is to discriminate between order and chaos. This distinction is a delicate issue because regular and chaotic orbits are distributed throughout phase space in very complicated ways. In order to address the problem several methods have been developed, which can be divided into two major categories: the ones based on the study of the evolution of deviation vectors from a given orbit, like the computation of the maximal Lyapunov characteristic exponent (mLCE) χ_1 [4], and those relying on the analysis of the particular orbit itself, like the frequency map analysis of Laskar [5].

Other chaos detection methods, belonging to the same category with the evaluation of the mLCE, are the fast Lyapunov indicator [6] and its variants [7], the smaller alignment index (SALI) [8] and its generalization, the so-called generalized alignment index (GALI) [9,10], and the mean exponential growth of nearby orbits [11]. The computation of these indicators requires the numerical integration of the so-called *variational equations*, which govern the time evolution of deviation vectors.

The scope of this paper is to present, analyze, and compare different numerical methods for the integration of the variational equations. In our study we consider methods based on symplectic and nonsymplectic integration techniques. The integration of the variational equations by nonsymplectic methods is straightforward since one simply has to integrate these equations simultaneously with the equations of motion. This approach requires, in general, more CPU time than schemes based on symplectic integration techniques for the same order of accuracy and integration time step. For this reason we *focus our attention on methods based on symplectic schemes*, explaining in detail their theoretical foundation and applying them to Hamiltonian systems of different numbers of degrees of freedom.

The numerical solution of the variational equations obtained by the various integration schemes studied are used for the computation of the spectrum of the Lyapunov characteristic exponents (LCEs) and the GALIs. We chose to compute these two chaos indicators among the indices based on the evolution of deviation vectors, because the computation of the mLCE is the elder and most commonly employed chaos detection technique, while the computation of the whole spectrum of LCEs and GALIs requires the evolution of more than one deviation vector and thus is strongly influenced by inaccuracies of the integration procedure. We investigate the numerical efficiency of the different integration methods by comparing the CPU times they require for the computation of the LCEs and the GALIs, as well as their accuracy in reproducing well-known properties of these chaos indicators. In particular, we check whether the set of computed LCEs consists of pairs of values having opposite signs and if the time evolution of GALIs follows specific theoretically predicted laws.

The paper is organized as follows: after introducing the concept of variational equations in the next section, we describe in Secs. III and IV the LCEs and the GALIs, respectively, which are the two chaos indicators we use in our study. Then, in Sec. V we give the basic properties of symplectic integrators. Section VI is devoted to the detailed description of several numerical schemes for the integration of the variational equations of Hamiltonian systems. Applications of these schemes to regular and chaotic orbits of systems with two or more degrees of freedom are presented in Sec. VII, where also the efficiency of each technique is discussed. Finally, in Sec. VIII, we summarize the results and present our conclusions, while in the Appendix the explicit

expressions of the various integration methods for the Hénon-Heiles system are given.

II. VARIATIONAL EQUATIONS

Let us consider an *autonomous Hamiltonian system* of N degrees of freedom (ND) having a Hamiltonian function

$$H(q_1,q_2,\ldots,q_N,p_1,p_2,\ldots,p_N)=h=\text{const}, \tag{1}$$

where q_i and p_i $(i=1,2,\ldots,N)$ are the generalized coordinates and conjugate momenta, respectively. An orbit in the $2N$-dimensional phase space $\mathcal{S}$ of this system is defined by the vector

$$\vec{x}(t)=(q_1(t),q_2(t),\ldots,q_N(t),p_1(t),p_2(t),\ldots,p_N(t)), \tag{2}$$

with $x_i=q_i$, $x_{i+N}=p_i$, and $i=1,2,\ldots,N$. The time evolution of this orbit is governed by the *Hamilton equations of motion*, which in matrix form are given by

$$\dot{\vec{x}}=\begin{bmatrix}\frac{\partial H}{\partial \vec{p}} & -\frac{\partial H}{\partial \vec{q}}\end{bmatrix}^{\mathrm{T}}=\mathbf{J}_{2N}\cdot\mathbf{D}_H, \tag{3}$$

with $\vec{q}=(q_1(t),q_2(t),\ldots,q_N(t))$, $\vec{p}=(p_1(t),p_2(t),\ldots,p_N(t))$, and

$$\mathbf{D}_H=\begin{bmatrix}\frac{\partial H}{\partial q_1} & \frac{\partial H}{\partial q_2} & \cdots & \frac{\partial H}{\partial q_N} & \frac{\partial H}{\partial p_1} & \frac{\partial H}{\partial p_2} & \cdots & \frac{\partial H}{\partial p_N}\end{bmatrix}^{\mathrm{T}},$$

with $(^{\mathrm{T}})$ denoting the transpose matrix. Matrix $\mathbf{J}_{2N}$ has the following block form:

$$\mathbf{J}_{2N}=\begin{bmatrix}\mathbf{0}_N & \mathbf{I}_N\\ -\mathbf{I}_N & \mathbf{0}_N\end{bmatrix},$$

with $\mathbf{I}_N$ being the $N\times N$ identity matrix and $\mathbf{0}_N$ being the $N\times N$ matrix with all its elements equal to zero.

An initial deviation vector $\vec{w}(0)=(\delta x_1(0),\delta x_2(0),\ldots,\delta x_{2N}(0))$ from an orbit $\vec{x}(t)$ evolves in the *tangent space* $\mathcal{T}_{\vec{x}}\mathcal{S}$ of $\mathcal{S}$ according to the so-called variational equations

$$\dot{\vec{w}}=[\mathbf{J}_{2N}\cdot\mathbf{D}_H^2(\vec{x}(t))]\cdot\vec{w}=:\mathbf{A}(t)\cdot\vec{w}, \tag{4}$$

with $\mathbf{D}_H^2(\vec{x}(t))$ being the Hessian matrix of Hamiltonian (1) calculated on the reference orbit $\vec{x}(t)$, i.e.,

$$\mathbf{D}_H^2(\vec{x}(t))_{ij}=\left.\frac{\partial^2 H}{\partial x_i\,\partial x_j}\right|_{\vec{x}(t)},\quad i,j=1,2,\ldots,2N.$$

Equations (4) are a set of linear differential equations with respect to $\vec{w}$, having time-dependent coefficients since matrix $\mathbf{A}(t)$ depends on the particular reference orbit, which is a function of time t.

In the present paper we consider autonomous Hamiltonians of the form

$$H(\vec{q},\vec{p})=\frac{1}{2}\sum_{i=1}^{N}p_i^2+V(\vec{q}), \tag{5}$$

with $V(\vec{q})$ being the potential function. The Hamilton equations of motion (3) become

$$\dot{\vec{x}}=\begin{bmatrix}\dot{\vec{q}}\\ \dot{\vec{p}}\end{bmatrix}=\begin{bmatrix}\vec{p}\\ -\frac{\partial V(\vec{q})}{\partial \vec{q}}\end{bmatrix}, \tag{6}$$

while the variational equations (4) of this system take the form

$$\dot{\vec{w}}=\begin{bmatrix}\dot{\vec{\delta q}}\\ \dot{\vec{\delta p}}\end{bmatrix}=\mathbf{A}(t)\cdot\vec{w}=\begin{bmatrix}\mathbf{0}_N & \mathbf{I}_N\\ -\mathbf{D}_V^2(\vec{q}(t)) & \mathbf{0}_N\end{bmatrix}\cdot\begin{bmatrix}\vec{\delta q}\\ \vec{\delta p}\end{bmatrix}\Rightarrow$$

$$\dot{\vec{\delta q}}=\vec{\delta p},\quad \dot{\vec{\delta p}}=-\mathbf{D}_V^2(\vec{q}(t))\,\vec{\delta q}, \tag{7}$$

with $\vec{\delta q}=(\delta q_1(t),\delta q_2(t),\ldots,\delta q_N(t))$, $\vec{\delta p}=(\delta p_1(t),\delta p_2(t)\ldots,\delta p_N(t))$, and

$$\mathbf{D}_V^2(\vec{q}(t))_{jk}=\left.\frac{\partial^2 V(\vec{q})}{\partial q_j\,\partial q_k}\right|_{\vec{q}(t)},\quad j,k=1,2,\ldots,N. \tag{8}$$

Thus, the tangent dynamics of Hamiltonian (5) is represented by the time-dependent Hamiltonian function

$$H_V(\vec{\delta q},\vec{\delta p};t)=\frac{1}{2}\sum_{i=1}^{N}\delta p_i^2+\frac{1}{2}\sum_{j,k}^{N}\mathbf{D}_V^2(\vec{q}(t))_{jk}\delta q_j\delta q_k, \tag{9}$$

which we call the *tangent dynamics Hamiltonian* (TDH) and whose equations of motion are exactly the variational equations (7).

III. LYAPUNOV CHARACTERISTIC EXPONENTS

The LCEs are asymptotic measures characterizing the average rate of growth (or shrinking) of small perturbations to the solutions of a dynamical system. Their concept was introduced by Lyapunov when studying the stability of nonstationary solutions of ordinary differential equations [12] and has been widely employed in studying dynamical systems since then. A detailed review of the theory of the LCEs, as well as of the numerical techniques developed for their computation can be found in [4].

The theory of LCEs was applied to characterize chaotic orbits by Oseledec [13], while the connection between LCEs and exponential divergence of nearby orbits was given in [14,15]. For a chaotic orbit at least one LCE is positive, implying exponential divergence of nearby orbits, while in the case of regular orbits all LCEs are zero or negative. Therefore, the computation of the mLCE χ_1 is sufficient for determining the nature of an orbit, because $\chi_1>0$ guarantees that the orbit is chaotic.

The mLCE is computed as the limit for $t\to\infty$ of the quantity

$$X_1(t)=\frac{1}{t}\ln\frac{\|\vec{w}(t)\|}{\|\vec{w}(0)\|}, \tag{10}$$

often called *finite-time mLCE*, where $\vec{w}(0)$ and $\vec{w}(t)$ are deviation vectors from a given orbit, at times $t=0$ and $t>0$, respectively, and $\|\cdot\|$ denotes the norm of a vector. So, we have

$$\chi_1 = \lim_{t\to\infty} X_1(t). \tag{11}$$

If the energy surface defined by Eq. (1) is compact, it has been shown that this limit is finite, independent of the choice of the metric for the phase space, and converges to χ_1 for almost all initial vectors $\vec{w}(0)$ [13,16,17]. $X_1(t)$ tends to zero in the case of regular orbits following a power law [14],

$$X_1(t) \propto t^{-1}, \tag{12}$$

while it tends to nonzero values in the case of chaotic orbits.

An ND Hamiltonian system has $2N$ (possibly nondistinct) LCEs, which are ordered as $\chi_1 \geq \chi_2 \geq \cdots \geq \chi_{2N}$. In [18] a theorem was formulated, which led directly to the development of a numerical technique for the computation of all LCEs, based on the time evolution of many deviation vectors, kept linearly independent through a Gram-Schmidt orthonormalization procedure. The theoretical framework, as well as the corresponding numerical method for the computation of all LCEs (usually called the *standard method*), was given in [16,17]. According to this method all other LCEs χ_2, χ_3, etc., apart from the mLCE obtained from Eq. (11), are computed as the limits for $t\to\infty$ of some appropriate quantities $X_2(t)$, $X_3(t)$, etc., which are called the *finite-time LCEs* (see [4,17] for more details). We note that throughout the present paper, whenever we need to compute the values of the LCEs, we apply the discrete QR-decomposition technique ([19], Sec. 2.10), which is a variation of the standard method (see Sec. 6.3 of [4] for more details).

It has been shown in [16] that in the case of an autonomous Hamiltonian flow, the set of LCEs consists of pairs of values having opposite signs,

$$\chi_i = -\chi_{2N-i+1}, \quad i = 1,2,\ldots,N. \tag{13}$$

In addition, since the Hamiltonian function is an integral of motion, at least two LCEs vanish, i.e.,

$$\chi_N = \chi_{N+1} = 0, \tag{14}$$

while the presence of any additional independent integral of motion leads to the vanishing of another pair of LCEs.

IV. GENERALIZED ALIGNMENT INDEX

The GALI is an efficient chaos detection technique introduced in [9] as a generalization of a similar indicator called the SALI [8]. The method has been applied successfully for the discrimination between regular and chaotic motions, as well as for the detection of regular motion on low-dimensional tori to different dynamical systems [10,20].

The GALI of order k (G_k) is determined through the evolution of $2\leq k\leq 2N$ initially linearly independent deviation vectors $\vec{w}_i(0)$ $(i=1,2,\ldots,k)$. The time evolution of each deviation vector is governed by the variational equations (7). Each evolved deviation vector $\vec{w}_i(t)$ is normalized from time to time, having its norm equal to 1, in order to avoid overflow problems, but its direction is left intact. Then, according to [9], G_k is defined to be the volume of the k-parallelogram having as edges the k unitary deviation vectors $\hat{w}_i(t)$ $(i=1,2,\ldots,k)$. This volume is equal to the norm of the wedge product of these vectors, and G_k is given by

$$G_k(t) = \|\hat{w}_1(t) \wedge \hat{w}_2(t) \wedge \cdots \wedge \hat{w}_k(t)\|. \tag{15}$$

From this definition it is evident that if at least two of the deviation vectors become linearly dependent, the wedge product in Eq. (15) becomes zero and G_k vanishes.

Expanding the wedge product (15) into a sum of determinants and studying the asymptotic behavior of those who vary the *slowest* in time, it is possible to show analytically the following [9]: in the case of a chaotic orbit all deviation vectors tend to become linearly dependent, aligning in the direction defined by the mLCE, and G_k tends to zero exponentially following the law

$$G_k(t) \propto e^{-[(\sigma_1-\sigma_2)+(\sigma_1-\sigma_3)+\cdots+(\sigma_1-\sigma_k)]t}, \tag{16}$$

where $\sigma_1,\ldots,\sigma_k$ are approximations of the first k largest Lyapunov exponents. On the other hand, in the case of regular motion on an N-dimensional torus, all deviation vectors tend to fall on the N-dimensional tangent space of this torus. Thus, if we start with $k\leq N$ general deviation vectors they will remain linearly independent on the N-dimensional tangent space of the torus, since there is no particular reason for them to become aligned. As a consequence G_k is different from zero and remains practically constant for $k\leq N$. On the other hand, G_k tends to zero for $k>N$ since some deviation vectors will eventually become linearly dependent, following a particular power law which depends on the dimensionality N of the torus and the number k of deviation vectors. The behavior of G_k for regular orbits lying on N-dimensional tori is given by

$$G_k(t) \propto \begin{cases} \text{const} & \text{if } 2 \leq k \leq N \\ \dfrac{1}{t^{2(k-N)}} & \text{if } N < k \leq 2N. \end{cases} \tag{17}$$

If the regular orbit lies on a low-dimensional torus, i.e., an s-dimensional torus with $2\leq s\leq N$, then G_k remains practically constant and different from zero for $k\leq s$ and tends to zero for $k>s$ following particular power laws (see [10] for more details).

In order to compute the value of G_k we consider the $2N\times k$ matrix $\mathbf{W}(t)$ having as columns the coordinates $w_{ji}(t)$ of the unitary deviation vectors $\hat{w}_i(t)$ (where $i=1,2,\ldots,k$ and $j=1,2,\ldots,2N$), with respect to the usual orthonormal basis $\hat{e}_1=(1,0,0,\ldots,0), \hat{e}_2=(0,1,0,\ldots,0),\ldots,\hat{e}_{2N}=(0,0,0,\ldots,1)$ of the $2N$-dimensional tangent space $\mathcal{T}_x S$ and perform the singular value decomposition of this matrix. Then, as it was shown in [10], G_k is equal to the product of the singular values z_i $(i=1,2,\ldots,k)$ of matrix $\mathbf{W}(t)$, i.e.,

$$G_k(t) = \prod_{i=1}^{k} z_i(t). \tag{18}$$

V. SYMPLECTIC INTEGRATORS

Let us discuss in some detail how we can integrate the equations of motion (3) of a general Hamiltonian (1) by a symplectic integration scheme, focusing our attention on a

particular family of integrators presented in [21]. Defining the Poisson bracket of functions $f(\vec{q},\vec{p})$ and $g(\vec{q},\vec{p})$ by [22]

$$\{f,g\} = \sum_{l=1}^{N} \left(\frac{\partial f}{\partial q_l}\frac{\partial g}{\partial p_l} - \frac{\partial f}{\partial p_l}\frac{\partial g}{\partial q_l} \right), \tag{19}$$

the Hamilton equations of motion (3) take the form

$$\frac{d\vec{x}}{dt} = \{\vec{x},H\} = L_H\vec{x}, \tag{20}$$

where L_H is the differential operator defined by $L_\chi f=\{f,\chi\}$. The solution of Eq. (20), for initial conditions $\vec{x}(0)=\vec{x}_0$, is formally written as

$$\vec{x}(t) = \sum_{n\geq 0} \frac{t^n}{n!} L_H^n \vec{x}_0 = e^{tL_H}\vec{x}_0. \tag{21}$$

Let us assume that the Hamiltonian function H can be split into two integrable parts as $H=A+B$. A symplectic scheme for integrating Eq. (20) from time t to time $t+\tau$ consists of approximating, in a symplectic way, the operator $e^{\tau L_H} = e^{\tau(L_A+L_B)}$ by an integrator of j steps involving products of operators $e^{c_i\tau L_A}$ and $e^{d_i\tau L_B}$ $(i=1,2,\ldots,j)$, which are exact integrations over times $c_i\tau$ and $d_i\tau$ of the integrable Hamiltonians A and B. The constants c_i and d_i, which in general can be positive or negative, are chosen to increase the order of the remainder of this approximation. So $e^{\tau L_A}$ and $e^{\tau L_B}$ are actually symplectic maps acting on the coordinate vector $\vec{x}$. Therefore, the integration of Eq. (20) over one time step τ, which evolves the initial coordinate vector $\vec{x}(t)$ to its final state $\vec{x}(t+\tau)$, is represented by the action on $\vec{x}(t)$ of a symplectic map S produced by the composition of products of $e^{c_i\tau L_A}$ and $e^{d_i\tau L_B}$. In this context several symplectic integrators of different orders have been developed by various researchers [23,24].

In [21] the families of SBAB (and SABA) symplectic integrators, which involve only forward (positive) integration steps were introduced. These integrators were adapted for the integration of perturbed Hamiltonians of the form $H=A+\epsilon B$, where both A and B are integrable and ϵ is a small parameter. A particular integrator SBAB_n (S_{Bn}), or SABA_n (S_{An}), involves n steps, i.e., n applications of products of $e^{c_i\tau L_A}$ and $e^{d_i\tau L_{\epsilon B}}$, and is of order $\mathcal{O}(\tau^{2n}\epsilon+\tau^2\epsilon^2)$ with respect to the integration step τ. This means that by using these integrators, we are actually approximating the dynamical behavior of the real Hamiltonian $A+\epsilon B$ by a Hamiltonian $H^* = A+\epsilon B+\mathcal{O}(\tau^{2n}\epsilon+\tau^2\epsilon^2)$, i.e., we introduce an error term of the order $\tau^{2n}\epsilon+\tau^2\epsilon^2$.

The accuracy of the S_{Bn} (S_{An}) integrator can be improved when the commutator term $C=\{B,\{B,A\}\}$ [25] leads to an integrable system, as in the common situation of A being quadratic in momenta $\vec{p}$ and B depending only on positions $\vec{q}$. In this case, two corrector terms of small backward (negative) steps can be added to the integrator S_{Bn},

$$S_{Bn}^c = e^{-\tau^3\epsilon^2(g/2)L_C}(S_{Bn})e^{-\tau^3\epsilon^2(g/2)L_C}. \tag{22}$$

A similar expression is valid also for S_{An}. The value of constant g is chosen in order to eliminate the $\tau^2\epsilon^2$ dependence of the remainder which becomes of order $\mathcal{O}(\tau^{2n}\epsilon+\tau^4\epsilon^2)$. The SBAB (SABA) integrators have already proved to be very efficient for the numerical study of different dynamical systems [21,26,27]. We note that several authors have used commutators for improving the efficiency of symplectic integrators (e.g., [28,29]).

Setting $\epsilon=1$ we can apply the SBAB (SABA) integration schemes for the integration of Hamiltonian (5) since this Hamiltonian can be written as $H=A+B$, with

$$A(\vec{p}) = \frac{1}{2}\sum_{i=1}^{N} p_i^2, \quad B(\vec{q}) = V(\vec{q}), \tag{23}$$

being both integrable. The maps $e^{\tau L_A}$ and $e^{\tau L_B}$, which propagate the set of initial conditions $(\vec{q},\vec{p})$ at time t to their final values $(\vec{q}',\vec{p}')$ at time $t+\tau$, for the Hamiltonian functions $A(\vec{p})$ and $B(\vec{q})$ [Eq. (23)] are

$$e^{\tau L_A}: \begin{cases} \vec{q}' = \vec{q} + \vec{p}\,\tau \\ \vec{p}' = \vec{p}, \end{cases} \tag{24}$$

$$e^{\tau L_B}: \begin{cases} \vec{q}' = \vec{q} \\ \vec{p}' = \vec{p} - \dfrac{\partial V(\vec{q})}{\partial \vec{q}}\tau, \end{cases} \tag{25}$$

respectively. For Hamiltonian (5) the corrector term is given by

$$C = \{B,\{B,A\}\} = \sum_{i=1}^{N} \left(\frac{\partial V(\vec{q})}{\partial \vec{q}_i} \right)^2, \tag{26}$$

which is a function of only the coordinates $\vec{q}$ and thus easily integrated as

$$e^{\tau L_C}: \begin{cases} \vec{q}' = \vec{q} \\ \vec{p}' = \vec{p} - \dfrac{\partial C(\vec{q})}{\partial \vec{q}}\tau. \end{cases} \tag{27}$$

In Appendix, Sec. 1 we give the explicit formulas of Eqs. (24), (25), and (27) for the Hénon-Heiles system (54).

VI. NUMERICAL INTEGRATION OF VARIATIONAL EQUATIONS

In this section we present several numerical schemes for the integration of the variational equations, considering both nonsymplectic techniques and methods based on symplectic integrators. The latter schemes are quite general and any symplectic integrator can be used for their implementation. In our study we consider an efficient fourth-order symplectic integrator, S_{B2}^c [21,28], which has an extra degree of complexity with respect to integrators composed of products of maps $e^{\tau L_A}$, and $e^{\tau L_B}$, since it requires the application of the corrector term C (26).

A. Nonsymplectic schemes

In order to follow the evolution of a deviation vector, the variational equations (7) have to be integrated simultaneously with the Hamilton equations of motion (6), since

matrix $\mathbf{D}_V^2(t)$ depends on the particular reference orbit $\vec{x}(t)$, which is a solution of Eq. (6). Any nonsymplectic numerical integration algorithm can be used for the integration of the whole set of equations (6) and (7).

In our study we use the DOP853 integration method which has been proven to be very efficient. The DOP853 integrator [30] is an explicit nonsymplectic Runge-Kutta integration scheme of order 8, based on the method of Dormand and Price (see [1], Sect. II.5). Two free parameters, τ and δ, are used to control the numerical performance of the method. The first one defines the time span between two successive outputs of the computed solution. After each step of length τ the values of LCEs (GALIs) are computed and the deviation vectors are orthonormalized (normalized). For the duration of each step τ, the integrator adjusts its own internal time step, so that the local one-step error is kept smaller than the user-defined threshold value δ. For DOP853 the estimation of this local error and the step size control is based on embedded formulas of orders 5 and 3.

B. Integration of the tangent dynamics Hamiltonian

Another approach to compute the evolution of deviation vectors is to initially integrate the Hamilton equations of motion (6), in order to obtain the time evolution of the reference orbit $\vec{x}(t)$, and then to use this numerically known solution for solving the equations of motion of the TDH (9), which are actually the variational equations (7). In practice one numerically solves the Hamilton equations of motion (6) by any (symplectic or nonsymplectic) integration scheme to obtain the values $\vec{x}(t_i)$ at $t_i=i\Delta t$ $(i=0,1,2,\ldots)$, where Δt is the integration time step of these orbits. Of course, the accuracy of the particular numerical scheme used for the construction of the time series $\vec{x}(t_i)$ will affect the quality of the numerical solution of the variational equations, regardless of the numerical scheme used for solving them. Having computed the values $\vec{x}(t_i)$ different methods can be applied for approximating the solution of the variational equations, which will be discussed in the following sections.

1. TDH with piecewise constant coefficients

One method is to approximate the actual time-dependent TDH (9) by a Hamiltonian with piecewise constant coefficients. This means assuming that the coefficients $\mathbf{D}_V^2(\vec{q}(t))_{jk}$ $(j,k=1,2,\ldots,N)$ of H_V (9) are constants equal to $\mathbf{D}_V^2(\vec{q}(t_i))_{jk}$ for the time interval $[t_i,t_i+\Delta t)$. These constants are determined by the values of the orbit's coordinates and are known since we know the time series $\vec{x}(t_i)=(\vec{q}(t_i),\vec{p}(t_i))$. Thus, for each time interval $[t_i,t_i+\Delta t)$ we end up with a quadratic form Hamiltonian function $H_V(\vec{\delta q},\vec{\delta p};t_i)$, whose equations of motion form a linear system of differential equations with constant coefficients.

The Hamiltonian $H_V(\vec{\delta q},\vec{\delta p};t_i)$ can be integrated by any symplectic or nonsymplectic integration scheme or can be explicitly solved by performing a canonical transformation to new variables $\vec{Q}$ and $\vec{P}$, so that the transformed Hamiltonian H_{VQP} becomes a sum of uncoupled one-dimensional Hamiltonians, whose equations of motion can be integrated immediately. To this end, let λ_k be the eigenvalues and $\vec{v}_k$ $(k=1,2,\ldots,N)$ be the unitary eigenvectors of the constant matrix $\mathbf{D}_V^2(\vec{q}(t_i))$. Then matrix $\mathbf{T}$, having as columns the eigenvectors $\vec{v}_k$, defines a canonical change of variables $\vec{q}=\mathbf{T}\vec{Q}$, $\vec{p}=\mathbf{T}\vec{P}$, which gives H_V the diagonal form

$$H_{VQP}=\sum_{i=1}^{N}\frac{1}{2}(P_i^2+\lambda_i Q_i^2). \tag{28}$$

The equations of motion of H_{VQP} are then easily solved.

In our study we use the same symplectic integrator (S_{B2}^c) both for obtaining the time series $\vec{x}(t_i)$ and for integrating the quadratic form Hamiltonian $H_V(\vec{\delta q},\vec{\delta p};t_i)$ in the time interval $[t_i,t_i+\Delta t)$. We name this approach the *TDHcc method* (cc means constant coefficients). An alternative approach is to compute the exact solution of the equations of motion of $H_V(\vec{\delta q},\vec{\delta p};t_i)$ (whose piecewise constant coefficients are obtained by the symplectic integration of the orbit using the S_{B2}^c scheme) by transforming it to a system of N uncoupled harmonic oscillators through the canonical transformation induced by matrix $\mathbf{T}$. This approach is called the *TDHes method* (es means exact solution).

In general, the transformation matrix $\mathbf{T}$ is determined for each time interval $[t_i,t_i+\Delta t)$ by solving numerically the eigenvalue problem

$$\mathbf{D}_V^2(\vec{q}(t_i))\vec{v}=\lambda\vec{v}, \tag{29}$$

a procedure which could become computationally very time consuming, especially for systems with many degrees of freedom. On the other hand, in some simple low-dimensional cases like, for example, the Hénon-Heiles system (54), the transformation matrix $\mathbf{T}$ can be determined analytically (see Appendix, Sec. 2a).

2. Integration of the TDH in an extended phase space

Instead of approximating H_V (9) by a quadratic form having constant coefficients for each time interval $[t_i,t_i+\Delta t)$, we can explicitly treat H_V as a time-dependent Hamiltonian. This time dependency is due to the fact that the coefficients of H_V are functions of the orbit's coordinates $\vec{q}(t)$. Like in the previous approach, we consider the time series $\vec{q}(t_i)$ to be known from the numerical integration of the Hamilton equations (6).

The ND time-dependent Hamiltonian H_V can be transformed to a time-independent Hamiltonian $\tilde{H}_V$ with an extra degree of freedom by considering the time t as an additional coordinate (see, for example, [31], Sec. 1.2b). For this purpose, we add to the Hamilton equations of motion of H_V the equations

$$\dot{t}=1, \quad \dot{H}_V=\frac{\partial H_V}{\partial t}. \tag{30}$$

Then we set t and $-H_V$ as additional coordinate and momentum, respectively, i.e., $\delta q_{N+1}=t$ and $\delta p_{N+1}=-H_V$, and define the new Hamiltonian

$$\tilde{H}_V(\vec{\xi},\vec{\eta}) = H_V(\vec{\delta q},\vec{\delta p};t) + \delta p_{N+1}, \tag{31}$$

where $\vec{\xi}=(\vec{\delta q},t)$ and $\vec{\eta}=(\vec{\delta p},-H_V)$ are, respectively, the new coordinates and momenta. The flow in the $(2N+2)$-dimensional extended phase space of the $(N+1)$D Hamiltonian $\tilde{H}_V$ is parametrized by a "new" time ζ such that $t(\zeta)=\zeta$, which does not appear explicitly in the functional form of $\tilde{H}_V$ (31). The set of equations (7) and (30) are the Hamilton equations of motion of $\tilde{H}_V$.

The dynamics of the ND TDH H_V (9) is equivalent to that of the $(N+1)$D Hamiltonian,

$$\tilde{H}_V(\vec{\delta q},t,\vec{\delta p},p_{N+1}) = \frac{1}{2}\sum_{j=1}^{N} \delta p_i^2 + \delta p_{N+1} + \frac{1}{2}\sum_{j,k}^{N} \mathbf{D}_V^2(\vec{q}(t))_{jk}\delta q_j \delta q_k. \tag{32}$$

This Hamiltonian can be easily integrated by any symplectic integration scheme since it can be split into two integrable parts:

$$\tilde{A}(\vec{\delta p},\delta p_{N+1}) = \frac{1}{2}\sum_{j=1}^{N} \delta p_i^2 + \delta p_{N+1},$$
$$\tilde{B}(\vec{\delta q},t) = \frac{1}{2}\sum_{j,k}^{N} \mathbf{D}_V^2(\vec{q}(t))_{jk}\delta q_j \delta q_k. \tag{33}$$

The maps $e^{\tau L_{\tilde{A}}}$ and $e^{\tau L_{\tilde{B}}}$, which propagate the set of initial conditions $(\vec{\delta q},t,\vec{\delta p},\delta p_{N+1})$ at time t to their final values $(\vec{\delta q}',t',\vec{\delta p}',\delta p'_{N+1})$ at time $t+\tau$, are

$$e^{\tau L_{\tilde{A}}}:\begin{cases} \vec{\delta q}' = \vec{\delta q} + \vec{\delta p}\,\tau \\ t' = t+\tau \\ \vec{\delta p}' = \vec{\delta p} \\ \delta p'_{N+1} = \delta p_{N+1}, \end{cases} \tag{34}$$

$$e^{\tau L_{\tilde{B}}}:\begin{cases} \vec{\delta q}' = \vec{\delta q} \\ t' = t \\ \vec{\delta p}' = \vec{\delta p} - \dfrac{\partial \tilde{B}(\vec{\delta q},t)}{\partial \vec{\delta q}}\tau \\ \delta p'_{N+1} = \delta p_{N+1} - \dfrac{\partial \tilde{B}(\vec{\delta q},t)}{\partial t}\tau. \end{cases} \tag{35}$$

The corrector term of the SBAB and SABA integration schemes,

$$\tilde{C} = \{\tilde{B},\{\tilde{B},\tilde{A}\}\} = \sum_{i=1}^{N}\left(\frac{\partial \tilde{B}(\vec{\delta q},t)}{\partial \vec{\delta q}_i}\right)^2, \tag{36}$$

is a function of only the coordinates $\vec{\xi}=(\vec{\delta q},t)$ and thus easily integrated,

$$e^{\tau L_{\tilde{C}}}:\begin{cases} \vec{\delta q}' = \vec{\delta q} \\ t' = t \\ \vec{\delta p}' = \vec{\delta p} - \dfrac{\partial \tilde{C}(\vec{\delta q},t)}{\partial \vec{\delta q}}\tau \\ \delta p'_{N+1} = \delta p_{N+1} - \dfrac{\partial \tilde{C}(\vec{\delta q},t)}{\partial t}\tau. \end{cases} \tag{37}$$

The explicit expressions of these maps for the Hénon-Heiles system (54) are given in Appendix, Sec. 2b.

From Eqs. (34), (35), and (37) we see that time t is changed only by the act of operator $e^{\tau L_{\tilde{A}}}$. On the other hand, operators $e^{\tau L_{\tilde{B}}}$ and $e^{\tau L_{\tilde{C}}}$ require the knowledge of positions $\vec{q}$ at specific times for the evaluation of the partial derivatives of $\tilde{B}$ and $\tilde{C}$. We also note that for all these operators the last equation for δp_{N+1} can be neglected since the knowledge of its value does not influence the evolution of the other quantities, and consequently the solution of the variational equations (7).

Since the coordinates of the orbit $\vec{q}$ are known only at specific times $t_i=i\Delta t$ $(i=0,1,\ldots)$, one is restricted to using integration schemes that require the knowledge of $\vec{q}$ at exactly these times. Such a scheme is, for example, the S_{B1} integrator

$$S_{B1} = e^{(\tau/2)L_{\tilde{B}}} e^{\tau L_{\tilde{A}}} e^{(\tau/2)L_{\tilde{B}}} \tag{38}$$

(which is practically the well-known Störmer/Verlet or leapfrog method) with $\tau=\Delta t$. The right operator $e^{(\tau/2)L_{\tilde{B}}}$ which acts first requires the knowledge of $\vec{q}(t_i)$, while the left operator $e^{(\tau/2)L_{\tilde{B}}}$ needs the values of $\vec{q}(t_i+\tau)=\vec{q}(t_{i+1})$, because the time value has changed from t_i to $t_i+\tau$ by $e^{\tau L_{\tilde{A}}}$. Note that the S_{A1} integrator,

$$S_{A1} = e^{(\tau/2)L_{\tilde{A}}} e^{\tau L_{\tilde{B}}} e^{(\tau/2)L_{\tilde{A}}}, \tag{39}$$

requires the knowledge of $\vec{q}(t_i+\tau/2)$ for the application of $e^{\tau L_{\tilde{B}}}$. This second-order integration scheme could be used with $\tau=2\Delta t$, leading in general to a less accurate algorithm compared to S_{B1} (38), which is also a second-order integrator but uses a smaller time step $\tau=\Delta t$. For $\tau=2\Delta t$ it is in general more efficient to apply the integration scheme

$$S_{B2} = e^{(\tau/6)L_{\tilde{B}}} e^{(\tau/2)L_{\tilde{A}}} e^{(2\tau/3)L_{\tilde{B}}} e^{(\tau/2)L_{\tilde{A}}} e^{(\tau/6)L_{\tilde{B}}}, \tag{40}$$

which was initially derived in [24]. This integrator needs the known values $\vec{q}(t_i)$, $\vec{q}(t_i+\tau/2)=\vec{q}(t_i+\Delta t)=\vec{q}(t_{i+1})$, and $\vec{q}(t_i+\tau)=\vec{q}(t_i+2\Delta t)=\vec{q}(t_{i+2})$.

The above integration schemes can also be combined with a corrector step since $e^{\tau L_{\tilde{C}}}$ (37) does not change the time values and acts before and after the main body of the integrator [see Eq. (22)], when t has values for which we know the coordinates $\vec{q}$. We refer to this technique as the *TDHeps method* (eps means extended phase space). For the numerical applications of the TDHeps method (presented in Sec. VII) we use the fourth-order integrator S_{B2}^c both for the integration of the variational equations and for the computation of the orbit.

Higher-order SBAB or SABA integrators cannot be used in this framework, because they require the knowledge of $\vec{q}$ at nonequidistant time values, different from t_i. In order to apply such schemes one could initially compute the solution of Eq. (6) also at these specific times (e.g., by interpolation), but this would lead to a cumbersome, complex, time consuming, and consequently inefficient scheme.

C. Tangent map method

The set of equations (6) and (7) can be considered as a unified set of differential equations

$$\left.\begin{aligned} \dot{\vec{q}} &= \vec{p} \\ \dot{\vec{p}} &= -\frac{\partial V(\vec{q})}{\partial \vec{q}} \\ \dot{\delta\vec{q}} &= \delta\vec{p} \\ \dot{\delta\vec{p}} &= -\mathbf{D}_V^2(\vec{q})\,\delta\vec{q} \end{aligned}\right\} \Rightarrow \frac{d\vec{u}}{dt} = L_{HV}\vec{u}, \tag{41}$$

where $\vec{u}=(\vec{q},\vec{p},\delta\vec{q},\delta\vec{p})$ is a vector formed by the phase-space vector $\vec{x}=(\vec{q},\vec{p})$ and the deviation vector $\vec{w}=(\delta\vec{q},\delta\vec{p})$, and L_{HV} is the differential operator of the whole system. In analogy to Eq. (21), the solution of system (41) for an initial condition $\vec{u}(0)$ can be formally written as $\vec{u}(t)=e^{tL_{HV}}\vec{u}(0)$. We describe now how symplectic integrators can be used to obtain this solution.

First of all, let us note that Eqs. (41) cannot be considered as the Hamilton equations of motion of some generalized Hamiltonian function. If such a Hamiltonian existed, and could be split into two integrable parts, any symplectic integrator could be used for finding the solution of system (41). Since this is not the case, we follow a different approach to achieve this goal. In Sec. V the integration of the equations of motion of Hamiltonian (5) over one integration time step τ was split into steps over appropriate time intervals $c_i\tau$ and $d_i\tau$, where the dynamics was determined either by Hamiltonian $A(\vec{p})$ or $B(\vec{q})$ [Eq. (23)]. During these intermediate steps the tangent dynamics of the system is governed by the variational equations

$$\dot{\delta\vec{q}} = \delta\vec{p}, \quad \dot{\delta\vec{p}} = 0, \tag{42}$$

for $A(\vec{p})$, and by

$$\dot{\delta\vec{q}} = 0, \quad \dot{\delta\vec{p}} = -\mathbf{D}_V^2(\vec{q})\,\delta\vec{q}, \tag{43}$$

for $B(\vec{q})$. Therefore, for each intermediate step of the symplectic integration scheme the dynamics of the phase and the tangent space is governed by sets of equations

$$\left.\begin{aligned} \dot{\vec{q}} &= \vec{p} \\ \dot{\vec{p}} &= 0 \\ \dot{\delta\vec{q}} &= \delta\vec{p} \\ \dot{\delta\vec{p}} &= 0 \end{aligned}\right\} \Rightarrow \frac{d\vec{u}}{dt} = L_{AV}\vec{u}, \tag{44}$$

$$\left.\begin{aligned} \dot{\vec{q}} &= 0 \\ \dot{\vec{p}} &= -\frac{\partial V(\vec{q})}{\partial \vec{q}} \\ \dot{\delta\vec{q}} &= 0 \\ \dot{\delta\vec{p}} &= -\mathbf{D}_V^2(\vec{q})\,\delta\vec{q} \end{aligned}\right\} \Rightarrow \frac{d\vec{u}}{dt} = L_{BV}\vec{u}, \tag{45}$$

for Hamiltonians $A(\vec{p})$ and $B(\vec{q})$ [Eq. (23)], respectively, with L_{AV} and L_{BV} being the corresponding differential operators.

These sets of equations are immediately solved, leading to maps

$$e^{\tau L_{AV}}:\begin{cases} \vec{q}\,' = \vec{q} + \vec{p}\,\tau \\ \vec{p}\,' = \vec{p} \\ \delta\vec{q}\,' = \delta\vec{q} + \delta\vec{p}\,\tau \\ \delta\vec{p}\,' = \delta\vec{p}, \end{cases} \tag{46}$$

$$e^{\tau L_{BV}}:\begin{cases} \vec{q}\,' = \vec{q} \\ \vec{p}\,' = \vec{p} - \dfrac{\partial V(\vec{q})}{\partial \vec{q}}\,\tau \\ \delta\vec{q}\,' = \delta\vec{q} \\ \delta\vec{p}\,' = \delta\vec{p} - \mathbf{D}_V^2(\vec{q})\,\delta\vec{q}\,\tau. \end{cases} \tag{47}$$

Obviously the first two equations of maps $e^{\tau L_{AV}}$ and $e^{\tau L_{BV}}$ are exactly maps $e^{\tau L_A}$ (24) and $e^{\tau L_B}$ (25), respectively.

Thus, *any symplectic integration scheme used to solve the Hamilton equations of motion (6), which involves the successive application of maps $e^{\tau L_A}$ (24) and $e^{\tau L_B}$ (25), can also be used for the simultaneous integration of the variational equations (7), i.e., for solving the set of equations (41), by replacing maps $e^{\tau L_A}$ and $e^{\tau L_B}$ with maps $e^{\tau L_{AV}}$ (46) and $e^{\tau L_{BV}}$ (47), respectively.* This statement is a specific application of a more general result which is stated, for example, in [21]: symplectic integration schemes can be applied to first-order differential systems $\dot{X}=LX$ that can be written in the form $\dot{X}=(L_A+L_B)X$, where L, L_A, and L_B are differential operators for which the two systems $\dot{X}=L_AX$ and $\dot{X}=L_BX$ are integrable. The system of differential equations $\dot{u}=L_{HV}u$ (41) belongs to this category since it can be split into the integrable systems $\dot{u}=L_{AV}u$ (44) and $\dot{u}=L_{BV}u$ (45).

Let us discuss this splitting in more detail. System (41) can be written as

$$\dot{\vec{\mathcal{Q}}} = \vec{\mathcal{P}}, \quad \dot{\vec{\mathcal{P}}} = \vec{\mathcal{F}}(\vec{\mathcal{Q}}), \tag{48}$$

with $\vec{\mathcal{Q}}=(\vec{q},\delta\vec{q})=(q_1,q_2,\ldots,q_N,\delta q_1,\delta q_2,\ldots,\delta q_N)$, $\vec{\mathcal{P}}=(\vec{p},\delta\vec{p})=(p_1,p_2,\ldots,p_N,\delta p_1,\delta p_2,\ldots,\delta p_N)$, and $\vec{\mathcal{F}}(\vec{\mathcal{Q}})$ being a vector with coordinates

$$\mathcal{F}_i = \begin{cases} -\dfrac{\partial V(\vec{q})}{\partial q_i} & \text{for } 1 \le i \le N \\ -\displaystyle\sum_{k=1}^{N} \frac{\partial^2 V(\vec{q})}{\partial q_i \partial q_k} \delta q_k & \text{for } N < i \le 2N. \end{cases} \tag{49}$$

Then the dynamics of any general variable $U(\vec{\mathcal{Q}},\vec{\mathcal{P}})$ is given by

$$\begin{aligned} \dot{U}(\vec{\mathcal{Q}},\vec{\mathcal{P}}) &= \sum_{i=1}^{2N} \left[\frac{\partial U(\vec{\mathcal{Q}},\vec{\mathcal{P}})}{\partial \mathcal{Q}_i} \dot{\mathcal{Q}}_i + \frac{\partial U(\vec{\mathcal{Q}},\vec{\mathcal{P}})}{\partial \mathcal{P}_i} \dot{\mathcal{P}}_i \right] \\ &\overset{(48)}{=} \left\{ \sum_{i=1}^{2N} \left[\mathcal{P}_i \frac{\partial}{\partial \mathcal{Q}_i} + \mathcal{F}_i \frac{\partial}{\partial \mathcal{P}_i} \right] \right\} U(\vec{\mathcal{Q}},\vec{\mathcal{P}}) \\ &= (L_{AV} + L_{BV}) U(\vec{\mathcal{Q}},\vec{\mathcal{P}}). \end{aligned} \tag{50}$$

The solution of Eq. (50) for a time step τ can be formally written as

$$U(t+\tau) = e^{\tau(L_{AV}+L_{BV})} U(t). \tag{51}$$

The decomposition of $e^{\tau(L_{AV}+L_{BV})}$ into products of operators $e^{\tau L_{AV}}$ and $e^{\tau L_{BV}}$ by any symplectic integration scheme gives rise to an exponential-splitting algorithm for the integration of system (41), which would be symplectic if Eqs. (41) were the equations of motion of a Hamiltonian function (which are not, as we have already discussed).

In our study we consider symplectic integrators that require the application of corrector terms. When the S^c_{Bn} (S^c_{An}) integrators are used, map $e^{\tau L_C}$ (27) acts for some intermediate steps of the algorithm. Formally one can consider that for these steps the phase-space dynamics is governed by the Hamilton equations of motion of the Hamiltonian function $C(\vec{q})$ (26) [whose solution is given by map $e^{\tau L_C}$ (27)]. Consequently, the tangent space dynamics is described for these time steps by the variational equations of Hamiltonian $C(\vec{q})$. So the evolution of the general vector $\vec{u}$ is given by

$$\left.\begin{aligned} \dot{\vec{q}} &= 0 \\ \dot{\vec{p}} &= -\frac{\partial C(\vec{q})}{\partial \vec{q}} \\ \dot{\delta\vec{q}} &= 0 \\ \dot{\delta\vec{p}} &= -\mathbf{D}^2_C(\vec{q})\,\delta\vec{q} \end{aligned}\right\} \Rightarrow \frac{d\vec{u}}{dt} = L_{CV}\vec{u}, \tag{52}$$

where $\mathbf{D}^2_C(\vec{q})_{jk} = \partial^2 C(\vec{q}) / \partial q_j \partial q_k$. We easily see that the solution of these equations is given by the map

$$e^{\tau L_{CV}}: \begin{cases} \vec{q}\,' = \vec{q} \\ \vec{p}\,' = \vec{p} - \dfrac{\partial C(\vec{q})}{\partial \vec{q}} \tau \\ \delta\vec{q}\,' = \delta\vec{q} \\ \delta\vec{p}\,' = \delta\vec{p} - \mathbf{D}^2_C(\vec{q})\,\delta\vec{q}\,\tau, \end{cases} \tag{53}$$

which, of course, is an extension of map $e^{\tau L_C}$ (27). So *the use of the corrector term with the S_{Bn} (S_{An}) integrator for the integration of system (41) requires the additional substitution of map $e^{\tau L_C}$ (27) by the extended map $e^{\tau L_{CV}}$ (53).*

We call the above-described procedure for the simultaneous integration of the Hamilton equations of motion (6) and the variational equations (7) the *tangent map (TM) method*. The explicit expressions of the extended maps $e^{\tau L_{AV}}$ (46), $e^{\tau L_{BV}}$ (47), and $e^{\tau L_{CV}}$ (53) for the Hénon-Heiles system (54) are given in Appendix, Sec. 2c.

VII. NUMERICAL APPLICATIONS

In order to study the efficiency of the different schemes for the integration of the variational equations, we apply them to some simple Hamiltonian systems of different numbers of degrees of freedom. In particular we consider (a) the well-known two-dimensional (2D) Hénon-Heiles system [32] described by the Hamiltonian

$$H_2 = \frac{1}{2}(p_x^2 + p_y^2) + \frac{1}{2}(x^2 + y^2) + x^2 y - \frac{1}{3}y^3, \tag{54}$$

(b) the three-dimensional (3D) Hamiltonian system

$$H_3 = \frac{1}{2}(x^2 + p_x^2) + \frac{\sqrt{2}}{2}(y^2 + p_y^2) + \frac{\sqrt{3}}{2}(z^2 + p_z^2) + x^2 y + x^2 z, \tag{55}$$

studied in [9,17,33], and (c) the famous Fermi-Pasta-Ulam (FPU) β-lattice model [34], which describes a chain of N particles with nearest-neighbor interaction, for the particular case of $N=8$ studied in [10]. The eight-dimensional (8D) Hamiltonian of this system is

$$H_8 = \sum_{i=1}^{8} \frac{p_i^2}{2} + \sum_{i=0}^{8} \left[\frac{(q_{i+1} - q_i)^2}{2} + \frac{\beta (q_{i+1} - q_i)^4}{4} \right]. \tag{56}$$

We consider some typical regular and chaotic orbits of these systems and investigate the efficiency of the various numerical techniques by checking how well their outcomes verify the following theoretically known properties of the LCEs and the GALIs:

(i) The finite-time mLCE $X_1(t)$ should eventually tend to zero in the case of regular orbits following the power law given in Eq. (12).

(ii) According to Eq. (13), the LCEs are grouped in pairs of values having opposite signs, and consequently their sum vanishes. Therefore, the same relation should be also satisfied by the limiting values of the corresponding finite-time LCEs, i.e.,

$$\lim_{t\to\infty} [X_i(t) + X_{2N-i+1}(t)] = 0, \quad i = 1,2,\ldots,N. \tag{57}$$

(iii) According to Eq. (14) at least two LCEs vanish, and therefore $X_N(t)$ and $X_{N+1}(t)$ should tend to zero.

(iv) The GALIs follow laws (16) and (17) for chaotic and regular orbits, respectively.

A. 2D Hénon-Heiles system

We implement first the various numerical schemes presented in Sec. VI for the integration of the variational equations of regular and chaotic orbits of the 2D Hénon-Heiles

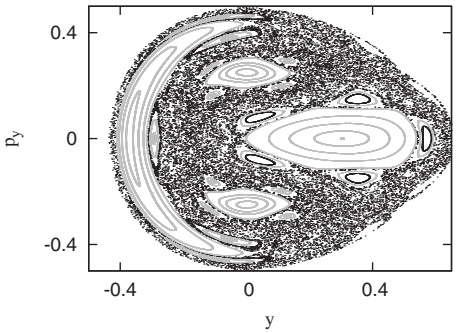

FIG. 1. The PSS defined by $x=0$, $p_x \geq 0$, for the Hénon-Heiles system (54) with $H_2=0.125$. The regular orbit R1 corresponds to the five closed black curves around the right large island of stability, while the chaotic orbit C1 is represented by the black dots scattered over the PSS. In order to get a clear picture of the structure of the whole PSS, other orbits of the system are plotted in gray.

system (54). The explicit expressions of all these schemes are presented in detail in Appendix, Sec. 2. The orbits of the Hénon-Heiles system have four LCEs $\chi_1 \geq \chi_2 \geq \chi_3 \geq \chi_4$, with $\chi_2=\chi_3=0$ and $\chi_1=-\chi_4 \geq 0$. A simple qualitative way of studying the dynamics of a Hamiltonian system is to plot the successive intersections of its orbits with a Poincaré surface of section (PSS) (see, for example, Sec. 1.2b of [31]). In 2D systems like Eq. (54), the PSS is a two-dimensional plane which allows the clear visualization of the dynamics.

In our study we keep the value of the Hamiltonian fixed at $H_2=0.125$. Initially, we consider two representative orbits of the system: the regular orbit R1 with initial conditions $x=0$, $p_x \approx 0.2334$, $y=0.558$, $p_y=0$, and the chaotic orbit C1 with initial conditions $x=0$, $p_x \approx 0.4208$, $y=-0.25$, $p_y=0$. In Fig. 1 we plot the intersection points of these two orbits with the PSS defined by $x=0$, $p_x \geq 0$. The points of the regular orbit lie on a torus and form five smooth closed curves (the so-called stability islands) on the PSS, while the points of the chaotic orbit appear randomly scattered.

First, we use the DOP853 nonsymplectic scheme to integrate the set of differential equations composed from the Hamilton equations of motion (A1) and the variational equations (A2). In our computations we set the integration time step $\tau=0.05$ and the threshold parameter $\delta=10^{-5}$, unless otherwise stated.

We also implement the TDHcc, the TDHes, and the TDHeps methods. For these methods we initially integrate Eqs. (A1) by the S^c_{B2} scheme. In this way we obtain the coordinates of the orbit at times $t_i=i\Delta t$ $(i=0,1,2,\ldots)$, with Δt being the constant integration step. Then we assume the TDH (A3) to have constant coefficients in each time interval $[t_i, t_i+\Delta t)$ and either we integrate in this interval its equations of motion by the S^c_{B2} integrator (TDHcc method) or we compute the exact solution of these equations by performing the canonical transformation induced by matrix $\mathbf{T}$ of Eq. (A10) (TDHes method). Alternatively, we use the S^c_{B2} scheme for integrating the equations of motion of the 3D Hamiltonian $\tilde{H}_{VH}$ (A13) in the time interval $[t_i, t_i+2\Delta t)$, by applying Eqs. (A15), (A16), and (A18) with time step $\tau=2\Delta t$ (TDHeps method). Finally, we implement the TM method using the S^c_{B2} integrator, which requires the application of maps (A21)–(A23).

As a final remark we note that in all the above-described schemes after each time step τ the LCEs (GALIs) are computed and the deviation vectors are orthonormalized (normalized) having a norm equal to 1.

1. Regular orbits

Results concerning the LCEs of the regular orbit R1 are shown in Fig. 2. In particular, the time evolution of the finite-time LCEs X_1 and X_2 is given in the upper panels, while in the lower panels the evolution of quantities $|X_1+X_4|$ and $|X_2+X_3|$ is plotted.

In Table I the information on the computation of the whole spectrum of LCEs of the R1 orbit up to $t=10^8$ is reported. The relative energy error, which could be consid-

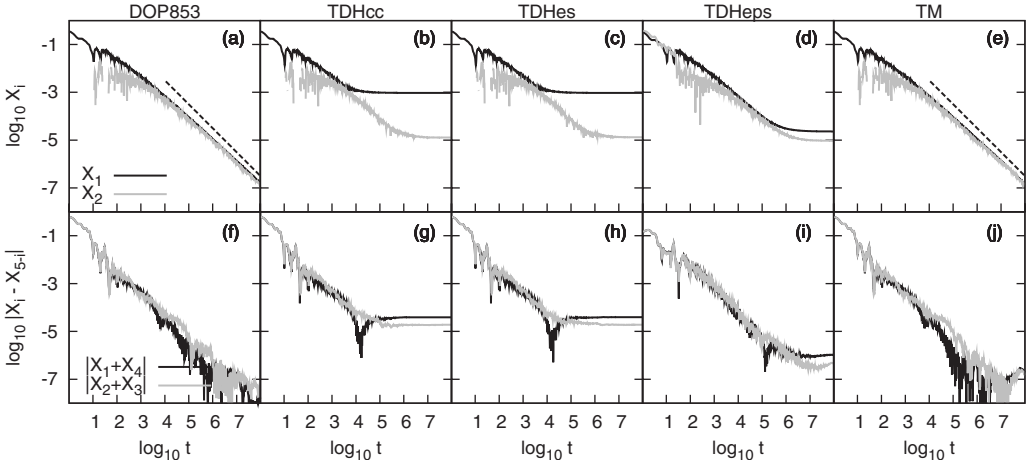

FIG. 2. The time evolution of $X_1(t)$ (black curves), $X_2(t)$ (gray curves) [upper panels] and $|X_1(t)+X_4(t)|$ (black curves), $|X_2(t)+X_3(t)|$ (gray curves) [lower panels] in log-log plots for the regular orbit R1 of the Hénon-Heiles system (54). The variational equations are integrated by [(a) and (f)] the DOP853 integrator, and by [(b) and (g)] the TDHcc, [(c) and (h)] the TDHes, [(d) and (i)] the TDHeps, and [(e) and (j)] the TM methods. Dashed lines in (a) and (e) correspond to functions proportional to t^{-1}. The step size is $\tau=0.05$ for all methods. For the DOP853 method the parameter $\delta=10^{-5}$ is used.

TABLE I. Information for the computation of the whole spectrum of LCEs for the regular orbit R1 of the Hénon-Heiles system (54), up to $t=10^8$. The nonsymplectic DOP853 algorithm and the symplectic S^c_{B2} integrator are used. In the latter case the S^c_{B2} scheme is used for the evolution of the orbit, while different approaches are applied for the integration of the variational equations. Step size τ is the time between two successive evaluations of the LCEs. For the TDHcc, the TDHes, and the TM methods, τ coincides with the integration time step Δt of the orbit, while for the TDHeps method $\tau=2\Delta t$. In the case of the DOP853 algorithm the integration over time τ is performed with a variable integration step, so that the local one-step error is kept smaller than δ. The relative energy error and the estimated value X_1 of the mLCE at $t=10^8$ are given. The required CPU time for the implementation of each method on an ordinary personal computer (AMD Athlon 1 GHz) is given in the last column. The first five cases are the ones presented in Fig. 2.

Integrator	Method	Step size τ	Relative energy error	X_1	CPU time
DOP853	$[\delta=10^{-5}]$	5×10^{-2}	7×10^{-10}	1.6×10^{-7}	8 h 18 min
S^c_{B2}	TDHcc	5×10^{-2}	2×10^{-8}	9.4×10^{-4}	5 h 48 min
S^c_{B2}	TDHes	5×10^{-2}	2×10^{-8}	9.4×10^{-4}	5 h 36 min
S^c_{B2}	TDHeps	5×10^{-2}	2×10^{-8}	2.3×10^{-5}	6 h 03 min
S^c_{B2}	TM	5×10^{-2}	2×10^{-8}	1.5×10^{-7}	4 h 40 min
DOP853	$[\delta=10^{-5}]$	1×10^{-1}	4×10^{-7}	1.6×10^{-7}	4 h 11 min
DOP853	$[\delta=10^{-10}]$	1×10^{-1}	4×10^{-7}	1.6×10^{-7}	4 h 12 min
DOP853	$[\delta=10^{-5}]$	2×10^{-1}	2×10^{-4}	2.4×10^{-7}	2 h 06 min
DOP853	$[\delta=10^{-10}]$	2×10^{-1}	2×10^{-4}	2.5×10^{-7}	2 h 03 min
DOP853	$[\delta=10^{-5}]$	5×10^{-1}	8×10^{-1}	1.1×10^{-6}	50 min
DOP853	$[\delta=10^{-10}]$	5×10^{-1}	6×10^{-4}	-7.7×10^{-8}	1 h 40 min
S^c_{B2}	TDHeps	1×10^{-1}	1×10^{-6}	8.9×10^{-5}	3 h 01 min
S^c_{B2}	TDHeps	2×10^{-1}	2×10^{-5}	3.5×10^{-4}	1 h 33 min
S^c_{B2}	TDHeps	5×10^{-1}	1×10^{-3}	1.8×10^{-3}	37 min
S^c_{B2}	TM	1×10^{-1}	2×10^{-6}	1.6×10^{-7}	2 h 16 min
S^c_{B2}	TM	2×10^{-1}	2×10^{-5}	3.3×10^{-8}	1 h 08 min
S^c_{B2}	TM	5×10^{-1}	1×10^{-3}	5.4×10^{-8}	27 min

ered as an indicator of the goodness of the integration procedure of orbit R1, increases with time for the DOP853 method, while it fluctuates around a constant value for all other methods. The values of this error and of X_1 at the end of the integration are reported in the table. The CPU time needed on an ordinary personal computer by each method for the integration of the equations of motion and the variational equations, as well as for the computation of the spectrum of LCEs, is also given.

The results of Fig. 2 show that the DOP853 [Fig. 2(a)] and the TM [Fig. 2(e)] methods have the best performance in evaluating the mLCE, because X_1 tends to zero until the end time $t=10^8$ of the integration, following a t^{-1} law. The good behavior of the DOP853 and the TM methods is due to the fact that the first technique is used for the integration of the actual set of equations (A1) and (A2) which govern the dynamics of the orbit and the deviation vector, while the second method approximates very accurately the dynamics of the system by the repeated application of a symplectic map, and the tangent dynamics by the act of the corresponding tangent map.

For the TDHcc [Fig. 2(b)], the TDHes [Fig. 2(c)], and the TDHeps [Fig. 2(d)] methods X_1 initially decreases too as $X_1 \propto t^{-1}$, but later its value deviates from the approximate t^{-1} law and tends to a constant (different for each method) non-zero value. Among these techniques the TDHeps method has the best performance, because the computed X_1 levels off to smaller values than in the cases of TDHcc and TDHes methods, being $X_1 \approx 2.3\times10^{-5}$ at $t=10^8$. Nevertheless, from the results of Figs. 2(b)–2(d) one would wrongly characterize the regular orbit R1 as chaotic. Concerning the TDHcc and TDHes methods, the main reason for this discrepancy is that these methods approximate the tangent dynamics by considering constants the actual time-dependent coefficients of Hamiltonian H_{VH} (A3), for the duration of each integration

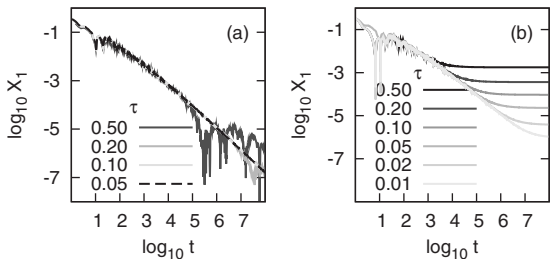

FIG. 3. The time evolution of $X_1(t)$ in log-log plots for the regular orbit R1 of the Hénon-Heiles system (54) for (a) the DOP853 (with $\delta=10^{-5}$) and (b) the TDHeps methods, when different step sizes τ are used. In (a) the curves for $\tau=0.05$ and $\tau=0.1$ practically overlap.

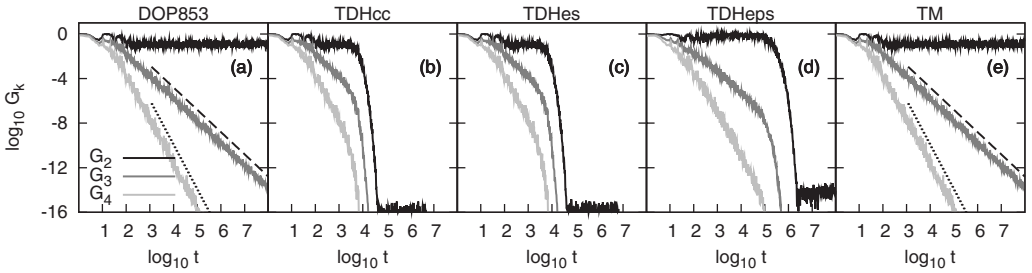

FIG. 4. The time evolution of $G_2(t)$ (black curves), $G_3(t)$ (gray curves), and $G_4(t)$ (light gray curves) for the regular orbit R1 of the Hénon-Heiles system (54). The variational equations are integrated by (a) the DOP853, (b) the TDHcc, (c) the TDHes, (d) the TDHeps, and (e) the TM methods. The plotted lines in (a) and (e) correspond to functions proportional to t^{-2} (dashed lines) and t^{-4} (dotted lines). The values of τ and δ used in the integrations are the same as in Fig. 2.

time step. The equations of motion of H_{VH} with constant coefficients are solved explicitly by the TDHes method, while their solution is approximated by the application of the TDHcc scheme. For the used time step $\tau=0.05$, both methods give practically the same X_1 at $t=10^8$. For smaller time steps the final values of X_1 obtained by both techniques are closer to the theoretical value $X_1=0$. On the other hand, since the TDHeps method takes into account the time-dependent nature of the coefficients of H_{VH}, it succeeds in obtaining a better estimation of the mLCE compared to the TDHcc and the TDHes methods.

The computed values of the second largest LCE ($\chi_2=0$) have similar characteristics with the results for the mLCE. Again, the finite-time LCE X_2 computed by the DOP853 integrator [Fig. 2(a)] and the TM method [Fig. 2(e)] tends to zero until the end of the integration time. On the other hand, X_2 computed by the TDHcc [Fig. 2(b)], the TDHes [Fig. 2(c)], and the TDHeps [Fig. 2(d)] methods does not tend to zero, but levels off to positive values which are always smaller than the level-off values of X_1. Again the TDHeps approach is more accurate, because the final value $X_2 \approx 9.3\times10^{-6}$ at $t=10^8$ obtained by this method is slightly smaller than the ones found by the TDHcc and the TDHes methods, and thus closer to the real $\chi_2=0$ value.

The ability of the DOP853 and the TM methods to evaluate quite accurately the LCEs of the regular orbit R1 is also shown by the tendency of quantities $|X_1+X_4|$ and $|X_2+X_3|$ to become zero [Figs. 2(f) and 2(j)]. Actually these quantities attain, for both methods, very small values of $\lesssim10^{-7}$ at $t=10^8$. But when these quantities are computed by the other three techniques they do not become zero as they theoretically should do, but level off to small positive values [Figs. 2(g)–2(i)]. Again the TDHeps method exhibits a better performance since the level-off values are smaller than the ones obtained by the TDHcc and the TDHes methods.

Looking in Table I at the CPU times needed for the computation of the whole spectrum of LCEs, one sees that the nonsymplectic method is the most expensive one. Among the remaining approaches the TM method is the fastest due to the fact that the whole set of equations for the evolution of both the orbit and the deviation vector are integrated together. The TDHcc and TDHes methods require more CPU time than the TM method, because for each integration time step the evolutions of the orbit and the deviation vectors are not performed simultaneously. First the orbit is evolved. Its coordinates define the coefficients of H_{VH} (A3), which are considered to be constant for the duration of the time step. Then, the deviation vectors are advanced for this particular Hamiltonian function for one time step. The TDHeps method needs even more CPU time mainly because the orbit is integrated with half time step ($\Delta t=\tau/2$) with respect to the other methods.

The first five rows of Table I contain information for the particular cases shown in Fig. 2. From these data we see that the energy error for the DOP853 method at $t=10^8$ is smaller than the error of the S^c_{B2} integrator used by the other methods. As it is also shown in Fig. 2 the values of X_1 obtained by the DOP853 and the TM methods are close to each other, despite the fact that the DOP853 method integrates orbit R1 with a better accuracy. Of major practical importance is the fact that the DOP853 method needs almost two times more CPU time than the TM method in order to compute the four LCEs up to $t=10^8$. Increasing the integration step size of DOP853 to $\tau=0.1$ [Fig. 3(a)] still permits the computation of the same X_1 value at $t=10^8$, but with a larger error in the conservation of H_2. The X_1 computed by the DOP853 method for even larger step sizes, such as $\tau=0.2$ and $\tau=0.5$, starts after some time to exhibit deviations from the $X_1 \propto t^{-1}$ law [Fig. 3(a)], leading to somewhat larger final values ($X_1 \approx 2.4\times10^{-7}$ for $\tau=0.2$ and $X_1 \approx 1.1\times10^{-6}$ for $\tau=0.5$) with respect to the $X_1 \approx 1.6\times10^{-7}$ value found for smaller τ. From our numerical experiments we see that the required CPU time for the DOP853 method, as well as the relative error of the computed energy H_2, mainly depends on the integration time step τ and not on the threshold parameter δ. In particular, for $\tau \lesssim 0.2$ the value of δ does not practically influence the required CPU time. For larger values of τ (for which nevertheless the obtained results are not very accurate) the CPU time is increased and the accuracy is improved when δ is decreased. On the other hand, the TM method succeeds even for $\tau=0.5$ to compute very fast the correct small final value of $X_1 \lesssim 10^{-7}$. This method keeps also the relative energy error at an acceptably low level, which is not the case any more for the DOP853 method with the same time step. Besides the computation speed, this is an additional advantage of the TM method over the DOP853 scheme.

It is worth noting that, although the DOP853 algorithm is an integration scheme of higher order than the S^c_{B2} symplectic integrator used in the TM method, it shows worse characteristics than the TM method, not only for large τ, but also

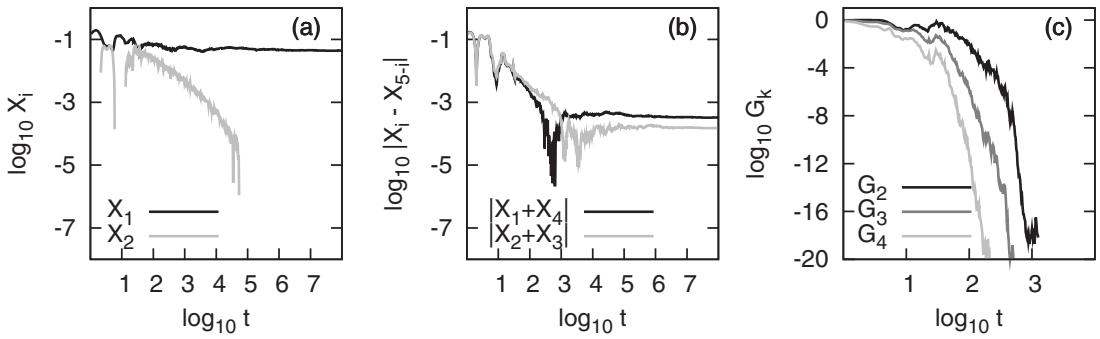

FIG. 5. The time evolution of (a) $X_1(t)$ (black curve), $X_2(t)$ (gray curve); (b) $|X_1(t)+X_4(t)|$ (black curve), $|X_2(t)+X_3(t)|$ (gray curve); and (c) $G_2(t)$ (black curve), $G_3(t)$ (gray curve), $G_4(t)$ (light gray curve) for the chaotic orbit C1 of the Hénon-Heiles system (54) when the variational equations are integrated by the DOP853 integrator. The values of τ and δ used in the integrations are the same as in Fig. 2.

when we compare implementations of the two algorithms that require almost the same CPU time. For example, the DOP853 method for $\tau=0.2$ and $\delta=10^{-10}$ (or even $\delta=10^{-5}$) has a final relative energy error which is larger by two orders of magnitude with respect to the error of the TM method for $\tau=0.1$ (which requires almost the same CPU time ≈ 2 h, as seen in Table I), and additionally the computed X_1 deviates from the $X_1 \propto t^{-1}$ law [Fig. 3(a)].

Among the other applied methods which wrongly characterize the R1 orbit as chaotic, the TDHeps scheme has the best performance since X_1 eventually levels off to a small positive value. From the results of Fig. 3(b) we see that the decrease in the step size τ pushes the starting time of the level-off to larger values and decreases the final value of X_1. So as one should expect, smaller integration steps result in a more accurate description of the evolution of the orbit and deviation vectors and leads to more accurate estimations of the LCEs. Nevertheless, the TM method is preferred over the TDHeps method because for the same step size τ it needs less CPU time, and additionally it estimates more accurately the LCEs.

For a regular orbit of the 2D Hamiltonian (54) and a random choice of initial deviation vectors, the theoretical prediction (17) for the behavior of the GALIs gives

$$G_2(t) \propto \text{const}, \quad G_3(t) \propto \frac{1}{t^2}, \quad G_4(t) \propto \frac{1}{t^4}. \tag{58}$$

In Fig. 4 we plot the time evolution of G_2, G_3, and G_4 for the regular orbit R1, when the variational equations are integrated by the same five numerical schemes used in Fig. 2. The results obtained by the DOP853 [Fig. 4(a)] and the TM [Fig. 4(e)] schemes are in accordance with the theoretical predictions (58). The GALIs computed by the TDHcc [Fig. 4(b)], the TDHes [Fig. 4(c)], and the TDHeps [Fig. 4(d)] methods follow the theoretical laws (58) up to $t \approx 10^4$ for the first two methods and up to $t \approx 10^5$ for the last one. After that time the GALIs fall exponentially fast to zero indicating, wrongly, that the orbit is chaotic. This behavior is in agreement with the behavior of X_1 obtained by these methods in Fig. 2, because the mLCE levels off to a positive value after some initial time interval, implying that the orbit is chaotic. The TDHeps method has again a better performance than the other two methods used to approximate the dynamics of the TDH (A3), since the computed GALIs follow the theoretical predictions (58) for longer times, but eventually it also fails to characterize correctly the nature of orbit R1.

2. Chaotic orbits

The computed LCEs and GALIs of the chaotic orbit C1 are practically the same irrespectively of which of the previously presented methods is used for the integration of the variational equations. For this reason in Fig. 5 we present results obtained only by the DOP853 integrator.

From the results of Fig. 5(a) we see that X_1 remains almost constant and different from zero, having practically the same value $X_1 \approx 4.5 \times 10^{-2}$ at $t=10^8$ for all applied schemes. Thus, all used methods are able to determine correctly the chaotic nature of the orbit. Since the Hénon-Heiles system (54) is conservative, $\chi_2=0$. From Fig. 5(a) we see that the finite-time LCE X_2 tends to zero and becomes negative after $t \approx 10^5$ with $|X_2| < 10^{-5}$. At that time all the applied numerical approaches reach their limits of applicability for the accurate computation of χ_2. The quantities $|X_1+X_4|$ and $|X_2+X_3|$ [Fig. 5(b)], which theoretically should be zero, level off after $t \approx 10^3 - 10^4$ to $|X_1+X_4| \approx 4 \times 10^{-4}$ and $|X_2+X_3| \approx 10^{-4}$ for all used schemes. This behavior indicates that all numerical methods succeed to revealing the symmetric nature of the spectrum of LCEs, but only up to four decimal digits of accuracy. Finally, the computed values of GALIs of orbit C1 [Fig. 5(c)] show an exponential decay to zero, which is a characteristic of chaoticity.

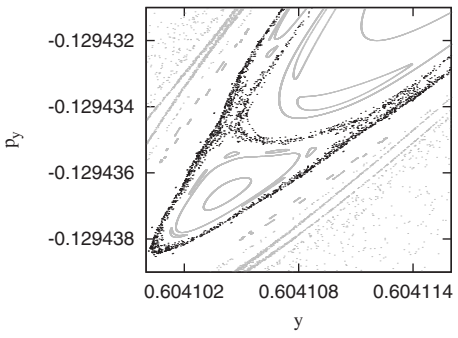

FIG. 6. A part of the PSS ($x=0$, $p_x \geq 0$) of the Hénon-Heiles system (54) with $H_2=0.125$, where the weakly chaotic orbit C2 is plotted by black dots.

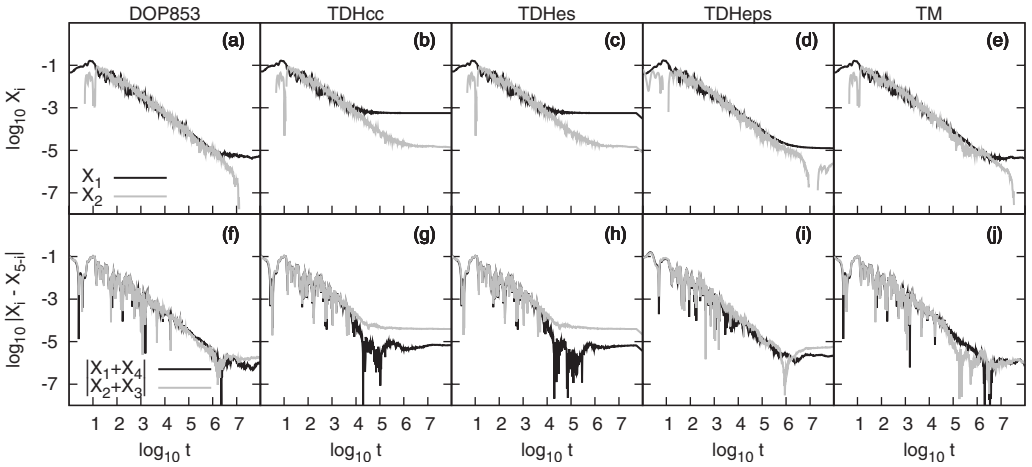

FIG. 7. The time evolution of $X_1(t)$ (black curves), $X_2(t)$ (gray curves) [upper panels] and $|X_1(t)+X_4(t)|$ (black curves), $|X_2(t)+X_3(t)|$ (gray curves) [lower panels] in log-log plots for the chaotic orbit C2 of the Hénon-Heiles system (54). The variational equations are integrated by [(a) and (f)] the DOP853 integrator, and by [(b) and (g)] the TDHcc, [(c) and (h)] the TDHes, [(d) and (i)] the TDHeps, and [(e) and (j)] the TM methods. The values of τ and δ used in the integrations are the same as in Fig. 2.

Figure 5 shows the equivalence of the different numerical techniques in the case of the chaotic orbit C1. This is a clear difference with respect to the behavior of the various numerical schemes for the regular orbit R1, where only the DOP853 and the TM methods gave similar (to each other) and correct results (Figs. 2 and 4). In order to check if the equivalence of all methods is valid for all chaotic orbits we consider a weakly chaotic orbit confined to a thin region of the phase space at the borders of a small stability island (Fig. 6). We call this orbit C2 and its initial conditions are $x=0$, $p_x \approx 0.11879$, $y=0.335\,036$, $p_y=-0.385\,631$.

From the results of the finite-time LCEs of orbit C2 presented in Fig. 7, we see that both the DOP853 [Fig. 7(a)] and the TM [Fig. 7(e)] methods characterize orbit C2 as weakly chaotic having a small mLCE $\chi_1 \approx 4\times 10^{-6}$. The TDHcc [Fig. 7(b)], the TDHes [Fig. 7(c)], and the TDHeps [Fig. 7(d)] methods also characterize orbit C2 as chaotic but overestimate the value of χ_1. Thus, these three methods fail to compute accurately the small value of the mLCE, with the TDHeps method showing once more the best performance, because the computed value ($X_1 \approx 1.3\times 10^{-5}$) is closer to the real value of χ_1. The limitations of these three methods are also clearly seen from the fact that the quantities $|X_1+X_4|$ and $|X_2+X_3|$ [Figs. 7(g)–7(i)] level off to larger values with respect to the results obtained by the DOP853 [Fig. 7(f)] and the TM [Fig. 7(j)] methods. It is worth noting that the level-off values of $|X_1+X_4|$ and $|X_2+X_3|$ obtained for orbit C2 by the DOP853 and the TM methods are smaller than the saturation values of the same quantities for the C1 orbit [Fig. 5(b)].

The results of Figs. 5 and 7 lead us to conclude that the DOP853 and the TM methods are able to accurately compute mLCEs for a larger range of χ_1 values than the TDHcc, the TDHes, and the TDHeps techniques. More specifically, our results show that the DOP853 and the TM schemes can evaluate χ_1 having values at least as small as 10^{-6}, while these small values definitely exceed the computational ability of the TDHeps method (which is the one with the best performance among the three other used methods) for the used step size τ.

The G_k ($k=2,3,4$) computed by the DOP853 [Fig. 8(a)] and the TM [Fig. 8(e)] methods has practically the same behavior. Up to $t \approx 10^6$, when the values of X_1 in Figs. 7(a) and 7(e) start to level off, deviating from the $X_1 \propto t^{-1}$ law, the GALIs follow the theoretical predictions (58) of regular motion. Later on the chaotic behavior of orbit C2 becomes prominent and the GALIs fall exponentially to zero. The time evolution of GALIs computed by the TDHcc [Fig. 8(b)], the TDHes [Fig. 8(c)], and the TDHeps [Fig. 8(d)] methods also indicates that the orbit is chaotic, but the exponential decay to zero starts earlier. This behavior is in accor-

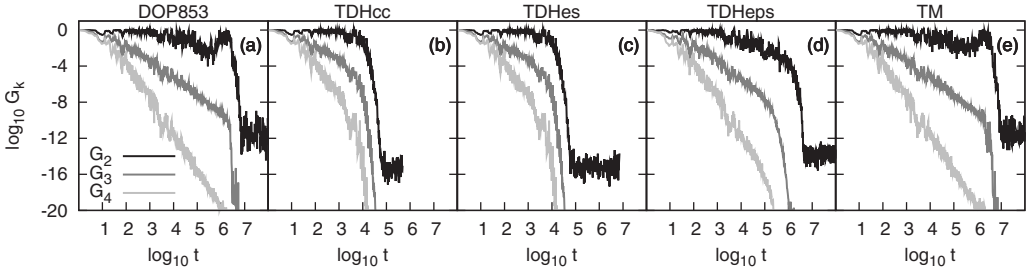

FIG. 8. The time evolution of $G_2(t)$ (black curves), $G_3(t)$ (gray curves), and $G_4(t)$ (light gray curves) for the chaotic orbit C2 of the Hénon-Heiles system (54). The variational equations are integrated by (a) the DOP853, (b) the TDHcc, (c) the TDHes, (d) the TDHeps, and (e) the TM methods. The values of τ and δ used in the integrations are the same as in Fig. 2.

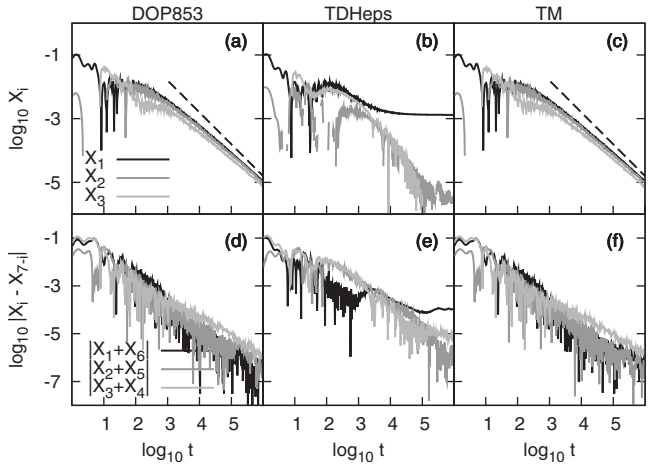

FIG. 9. The time evolution of $X_1(t)$, $X_2(t)$, $X_3(t)$ (upper panels) and $|X_1(t)+X_6(t)|$, $|X_2(t)+X_5(t)|$, $|X_3(t)+X_4(t)|$ (lower panels) in log-log plots for the regular orbit R2 of the 3D Hamiltonian system (55). The variational equations are integrated by [(a) and (d)] the DOP853 integrator, and by [(b) and (e)] the TDHeps and [(c) and (f)] the TM methods. The step size is $\tau=0.05$ for all methods. For the DOP853 method the parameter $\delta=10^{-5}$ is used. Dashed lines in (a) and (c) correspond to functions proportional to t^{-1}.

dance with the overestimation of orbit's chaoticity, which was also seen in the computation of X_1 [Figs. 7(b)–7(d)].

B. Hamiltonian systems with more than two degrees of freedom

Let us now apply the five different methods used in Sec. VII A to regular and chaotic orbits of the 3D and the 8D Hamiltonian systems (55) and (56). In all studied cases the computed LCEs and the GALIs have similar characteristics to the ones seen for the 2D system (54). Due to the fact that the TM, the DOP853, and the TDHeps methods always exhibited the best numerical performance, we present in this section results obtained only by these methods for the case of regular orbits.

In Fig. 9 we show results for the six LCEs of a regular orbit with initial conditions $x=y=z=0$, $p_x=0.1$, $p_y=0.347$, $p_z=0$ (orbit R2) of the 3D system (55), which was also studied in [9]. Similarly to the results obtained for the 2D regular orbit R1 in Fig. 2, the three largest finite-time LCEs X_1, X_2, and X_3 computed by the DOP853 [Fig. 9(a)] and the TM [Fig. 9(c)] methods tend to zero following a $X_i \propto t^{-1}$ $(i=1,2,3)$ law, which indicates the regular nature of the orbit. These two methods are also able to determine the symmetric nature of the spectrum of LCEs since the quantities $|X_1(t)+X_6(t)|$, $|X_2(t)+X_5(t)|$, and $|X_3(t)+X_4(t)|$ tend to zero [Figs. 9(d) and 9(f)]. On the other hand, using the TDHeps method one would again wrongly characterize the orbit as chaotic because the computed X_1 levels off at $t\approx 10^4$ to a positive value, being $X_1 \approx 1.3\times 10^{-3}$ at $t=10^6$ [Fig. 9(b)]. X_2 and X_3 show a better convergence to zero, while the latter one becomes negative after $t\approx 10^5$ with $|X_3|<10^{-5}$. In addition, the quantity $|X_1(t)+X_6(t)|$ levels off to some finite value, while $|X_2(t)+X_5(t)|$ and $|X_3(t)+X_4(t)|$ continue to approach zero until the end of the integration [Fig. 9(e)].

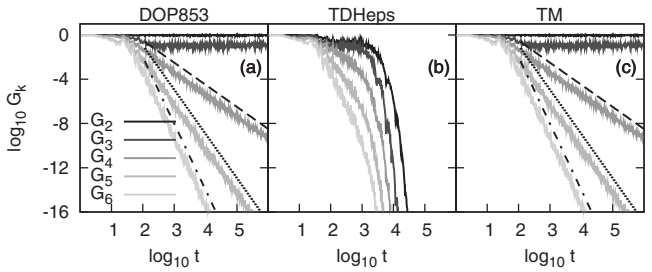

FIG. 10. The time evolution of $G_k(t)$ $(k=2,3,\ldots,6)$ for the regular orbit R2 of the 3D Hamiltonian system (55). The variational equations are integrated by (a) the DOP853, (b) the TDHeps, and (c) the TM methods. The values of τ and δ used in the integrations are the same as in Fig. 9. The plotted lines in (a) and (c) correspond to functions proportional to t^{-2} (dashed line), t^{-4} (dotted line), and t^{-6} (dashed-dotted line).

According to Eq. (17) the GALIs of a regular orbit of the 3D Hamiltonian system (55) should evolve as

$$G_2(t) \propto \text{const}, \quad G_3(t) \propto \text{const},$$
$$G_4(t) \propto \frac{1}{t^2}, \quad G_5(t) \propto \frac{1}{t^4}, \quad G_6(t) \propto \frac{1}{t^6}. \tag{59}$$

This behavior is seen for orbit R2 in Figs. 10(a) and 10(c) where the DOP853 and the TM methods are used, respectively, for the integration of the variational equations. Similarly to the case of regular orbit R1 (Fig. 4) the GALIs indicate that the orbit is regular. On the other hand, in Fig. 10(b) where the TDHeps method is applied, the computed GALIs eventually show an exponential decay, wrongly suggesting that orbit R2 is chaotic.

Finally, let us consider a particular regular orbit of the 8D Hamiltonian system (56) which lies on a low-dimensional torus. In our study we impose fixed boundary conditions, i.e., $q_0(t)=q_9(t)=p_0(t)=p_9(t)=0$ for all times t, fix the system's parameter to $\beta=1.5$, and consider the regular orbit with initial conditions $q_i=0.1$, $p_i=0$ $(i=1,2,\ldots,8)$, which we call orbit R3. This orbit lies on a four-dimensional torus and was also studied in [10].

According to the theory of GALIs developed in [10], regular motion on a four-dimensional torus implies that the corresponding G_2, G_3, and G_4 remain practically constant, while the remaining indices up to G_{16} tend to zero following particular power laws (see also Fig. 4 of [10]). As we can see from Fig. 11, these expected behaviors are well reproduced when the DOP853 [Figs. 11(a) and 11(d)] and the TM [Figs. 11(c) and 11(f)] methods are used for the integration of the variational equations. On the other hand, the TDHeps method fails to clearly determine the regular nature of orbit R3, as well as the dimensionality of the torus on which the orbit lies. From Figs. 11(b) and 11(e) we see that the computed GALIs have a behavior similar to the one obtained by the DOP853 and the TM methods, which indicates the regularity of the orbit, but only up to $t\approx 10^5$. For $t>10^5$ the computed GALIs eventually show an exponential decay, wrongly suggesting that the orbit is chaotic.

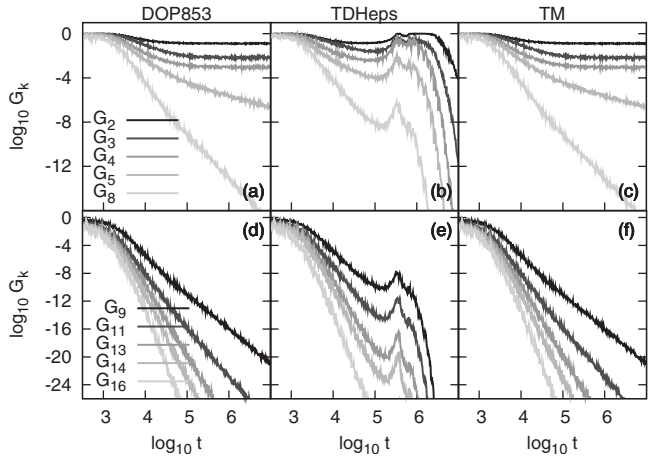

FIG. 11. The time evolution of $G_k(t)$, with $k=2,3,4,5,8$ (upper panels) and $k=9,11,13,14,16$ (lower panels) for the regular orbit R3 of the 8D Hamiltonian system (56). The variational equations are integrated by [(a) and (d)] the DOP853, [(b) and (e)] the TDHeps, and [(c) and (f)] the TM methods. The step size is $\tau=0.02$ for all methods. For the DOP853 method the parameter $\delta=10^{-5}$ is used.

VIII. SUMMARY AND DISCUSSION

We considered the problem of the accurate and fast integration of the variational equations of autonomous Hamiltonian systems. These equations govern the evolution of a deviation vector from an orbit of the system. The reliable determination of this evolution is necessary when studies of the chaotic behavior of the system are needed. Many chaos detection techniques, such as the LCEs and the GALIs which we considered in our study, are based on the evolution of one or more deviation vectors.

We made a detailed presentation of several numerical schemes for the integration of the variational equations, and we applied them to regular and chaotic orbits of Hamiltonian systems with different numbers of degrees of freedom. We also investigated the efficiency of these methods by comparing the CPU times they need for the computation of the spectrum of LCEs, as well as their ability to accurately reproduce well-known properties of the LCEs and the GALIs.

The evolution of deviation vectors cannot be separated from the evolution of the orbit itself because the explicit expression of the variational equations depends on the solution of the Hamilton equations of motion. Therefore, any general-purpose integration scheme for ordinary differential equations, like the DOP853 integrator we considered in our study, can be used for the simultaneous integration of the set of equations which includes both the Hamilton equations of motion and the variational equations. This method proved to be very reliable since it reproduced correctly the behavior of the LCEs and the GALIs for all tested orbits and systems.

When the Hamiltonian function H can be split into two integrable parts A and B, like $H=A+B$, symplectic integrators can be used for the integration of the equations of motion. Symplectic integrators are known to have better performance than nonsymplectic ones for the same integration time step, in terms of accuracy and required CPU time. In order to investigate the applicability of such methods for the integration of the variational equations, we focused our study explicitly on Hamiltonians of the form $H=A+B$. In particular, we considered Hamiltonians having a kinetic energy which is quadratic in the momenta and a potential which depends only on the positions [Eq. (5)]. For such systems the two integrable parts A and B are usually chosen to be the kinetic energy and the potential, respectively. Most symplectic schemes require the construction of symplectic maps $e^{\tau L_A}$ (24) and $e^{\tau L_B}$ (25) for the solution of the integrable parts A and B. In our study we considered a very efficient symplectic method, the S^c_{B2} integrator, which has an extra degree of complexity with respect to most symplectic integrators, since it requires the explicit solution of an additional corrector term C [map $e^{\tau L_C}$ (27)].

The variational equations of Hamiltonian (5) can be written as the Hamilton equations of motion of the time-dependent TDH (9), whose coefficients are defined by the coordinates of the orbit. Although individually the Hamilton equations of motion (6) and the variational equations (7) are equations of motion of Hamiltonian functions, system (41) which includes together both of them cannot be considered as the equations of motion of a new generalized Hamiltonian, and so symplectic integrators cannot be directly used for solving it. In our study we applied several approaches based on symplectic techniques for the integration of the variational equations. One approach we considered was the approximation of the solution of the TDH through the knowledge of the orbit's coordinates at specific times. These coordinates can be obtained by any symplectic or nonsymplectic integrator, independent of the method we use for approximating the solution of the variational equations. In our study we applied the S^c_{B2} integrator for this purpose. First we assumed the coefficients of the TDH to be constants for each integration step, and we integrated the resulting quadratic TDH by the S^c_{B2} integrator (TDHcc method) or solved it explicitly (TDHes method) whenever this was possible [like, for example, in the case of the Hénon-Heiles system (54)]. An alternative way we also implemented was to use the S^c_{B2} integrator for integrating the time-dependent TDH in an extended phase space (TDHeps method), using again the knowledge of orbit's coordinates at specific times. As an application of the TDHeps method we refer to the numerical study of the FPU problem in [35] where a leap-frog integrator was used for the integration of the time-dependent TDH.

The TDHcc, the TDHes, and the TDHeps methods had a rather poor numerical performance as they failed in many cases to determine correctly the regular or chaotic nature of orbits. Our numerical results show that the computed values of the LCEs cannot become smaller than a small positive value, which sets a lower limit to the ability of these techniques to numerically determine very small LCEs. So, one could wrongly characterize regular orbits as slightly chaotic because their computed LCEs cannot become smaller than the above-mentioned limit, although their actual LCEs are zero. This happens for the regular orbits R1 (Fig. 2) and R2 (Fig. 9). Of course this limiting value decreases for smaller integration steps because the numerical schemes approximate better the real tangent dynamics of the system [Fig. 3(b)]. Additionally, one could overestimate the mLCE of chaotic orbits like, for example, in the case of the chaotic

orbit C2 (Fig. 7). Nevertheless, these methods always required less CPU time than the nonsymplectic DOP853 method for the same time step. Therefore, these schemes can be used for some rough and fast evaluation of LCEs' charts, but not for the detailed investigation of the dynamics or for the accurate computation of the LCEs and GALIs. We note that among these three techniques the TDHeps method had always the best numerical performance, although it required a bit more CPU time than the other two methods.

The use of any symplectic scheme for the integration of the equations of motion (6) of the ND Hamiltonian (5) corresponds to the repeated action of a $2N$-dimensional symplectic map S, constructed by the appropriate composition of maps $e^{\tau L_A}$ (24) and $e^{\tau L_B}$ (25) [and $e^{\tau L_C}$ (27) if the corrector term C is used]. Then, the tangent dynamics of the flow, i.e., the solution of the variational equations (7), is described by the tangent map $TS=\partial S/\partial \vec{x}$ of S (some particular implementations of this approach for different physical problems can be found in [36,37]).

The TM method we presented in our study provides a simple systematic technique to construct the tangent map TS for any general symplectic integration scheme used for the integration of the orbit, which is perfectly suited for practical implementations. According to this method, one has to substitute the $2N$-dimensional maps $e^{\tau L_A}$ (24), $e^{\tau L_B}$ (25), and $e^{\tau L_C}$ (27) needed for the symplectic integration of the equations of motion (6) by the extended $4N$-dimensional maps $e^{\tau L_{AV}}$ (46), $e^{\tau L_{BV}}$ (47), $e^{\tau L_{CV}}$ (53), respectively. This procedure leads to the construction of an extended $4N$-dimensional final map composed by the $2N$-dimensional maps S and TS. In particular, the first $2N$ equations of this map are the equations of map S, and the rest $2N$ equations form the tangent map TS.

The TM method and the DOP853 integrator were the only techniques that succeeded in computing correctly the LCEs and the GALIs for all studied cases. Among them, the TM method required less CPU time for the same integration step size. Another advantage of the TM method over the DOP853 integrator is that its application with larger time steps reduces the needed CPU time, keeps the accuracy to acceptable levels, and produces more reliable results than the DOP853 integrator.

In conclusion, the TM method proved to be the most efficient one among all tested methods since it required the least CPU time for the computation of the spectrum of LCEs and reproduced very accurately the behavior of the LCEs and GALIs. Therefore, whenever the studied Hamiltonian can be split into two integrable parts, so that it can be integrated by symplectic integrators, the TM method should be preferred over other symplectic or nonsymplectic integration schemes.

Although we considered in our study applications of the TM method to Hamiltonian systems of relatively low dimensionality (systems having up to eight degrees of freedom), the method is expected to be also very efficient for higher-dimensional systems. Symplectic integrators have already been applied successfully for the accurate integration of motion in multidimensional systems which are related, for example, to problems of astronomical interest (e.g., [37]), of molecular dynamics (e.g., [29,38]), and dynamics of nonlinear lattices (e.g., [27]). Using the TM method these symplectic integration schemes can be extended to integrate also the corresponding variational equations. This is a problem of great practical importance, which we plan to address in a future publication.

As a final remark, we note that all the presented methods require the knowledge of the analytical expression of matrix $\mathbf{D}_V^2(\vec{q}(t))$ (8) [or of matrix $\mathbf{A}(t)$ (4) in the case of a general dynamical system]. If the variational equations cannot be written explicitly, possibly due to the complicated form of the studied dynamical system, the analytical derivation of these matrices is not possible and their elements could be estimated numerically, introducing an additional error to the solution of the variational equations. An approach that could be followed in such cases is the approximation of the solution of the variational equations by the difference of two orbits initially located very close to each other (see [39] for some particular applications of this approach). This is the so-called *two-particle method*, which was introduced in [14] and is mainly used for the evaluation of the mLCE. It was realized almost immediately after the introduction of this technique that this approach is less efficient and reliable than the actual integration of the variational equations [33] (whenever, of course, this integration is possible). For this reason we did not include this approach in our study.

ACKNOWLEDGMENTS

Ch. S. would like to thank G. Benettin, J. Bodyfelt, T. Bountis, T. Kovács, J. Laskar, and A. Ponno for useful discussions. E.G. acknowledges financial support by the DFG Project No. SO 216/21-1. We would also like to thank the anonymous referees for very useful comments and suggestions which helped us improve the clarity of the paper.

APPENDIX: ANALYTICAL EXPRESSIONS FOR THE INTEGRATION OF THE HÉNON-HEILES SYSTEM

We present here the explicit expressions of the various integration schemes for the 2D Hénon-Heiles system, whose Hamiltonian function (54) is of form (5) with $\vec{q}=(x,y)$ and $\vec{p}=(p_x,p_y)$. The Hamilton equations of motion (6) are

$$\begin{aligned} \dot{x} &= p_x, \\ \dot{y} &= p_y, \\ \dot{p}_x &= -x - 2xy, \\ \dot{p}_y &= y^2 - x^2 - y. \end{aligned} \tag{A1}$$

The variational equations (7) of the system are

$$\begin{aligned} \dot{\delta x} &= \delta p_x, \\ \dot{\delta y} &= \delta p_y, \\ \dot{\delta p}_x &= -(1+2y)\delta x - 2x\delta y, \\ \dot{\delta p}_y &= -2x\delta x + (-1+2y)\delta y, \end{aligned} \tag{A2}$$

while the corresponding TDH (9) takes the form

$$H_{VH}(\delta x, \delta y, \delta p_x, \delta p_y; t) = \tfrac{1}{2}(\delta p_x^2 + \delta p_y^2) + \tfrac{1}{2}\{[1 + 2y(t)]\delta x^2 + [1 - 2y(t)]\delta y^2 + 2[2x(t)]\delta x \delta y\}. \quad \text{(A3)}$$

1. Symplectic integration of the equations of motion

The Hénon-Heiles Hamiltonian (54) can be split into two parts $H_2 = A + B$, according to Eq. (23), with

$$A = \tfrac{1}{2}(p_x^2 + p_y^2), \quad B = \tfrac{1}{2}(x^2 + y^2) + x^2 y - \tfrac{1}{3}y^3. \quad \text{(A4)}$$

As it was explained in Sec. V, this separation is convenient for the application of symplectic schemes for the integration of Eqs. (A1) since Hamiltonians A and B are integrable. The maps $e^{\tau L_A}$ (24) and $e^{\tau L_B}$ (25), which propagate the set of initial conditions (x, y, p_x, p_y) at time t to their final values (x', y', p_x', p_y') at time $t + \tau$, are

$$e^{\tau L_A}: \begin{cases} x' = x + p_x \tau \\ y' = y + p_y \tau \\ p_x' = p_x \\ p_y' = p_y, \end{cases} \quad \text{(A5)}$$

$$e^{\tau L_B}: \begin{cases} x' = x \\ y' = y \\ p_x' = p_x - x(1 + 2y)\tau \\ p_y' = p_y + (y^2 - x^2 - y)\tau. \end{cases} \quad \text{(A6)}$$

The corrector term (26) is

$$C = \{B, \{B, A\}\} = (x + 2xy)^2 + (x^2 - y^2 + y)^2, \quad \text{(A7)}$$

and the corresponding map $e^{\tau L_C}$ (27) is

$$e^{\tau L_C}: \begin{cases} x' = x \\ y' = y \\ p_x' = p_x - 2x(1 + 2x^2 + 6y + 2y^2)\tau \\ p_y' = p_y - 2(y - 3y^2 + 2y^3 + 3x^2 + 2x^2 y)\tau. \end{cases} \quad \text{(A8)}$$

2. Integration of the variational equations

We derive now for the particular case of the Hénon-Heiles system the analytical expressions of the various numerical schemes presented in Sec. VI for the integration of the variational equations.

a. Diagonal form of the TDH (A3) with constant coefficients. Inserting the values $x(t_i) \equiv x_i$ and $y(t_i) \equiv y_i$ at a specific time t_i in the functional form of the TDH (A3), H_{VH} becomes a quadratic 2D Hamiltonian with constant coefficients. The equations of motion of this Hamiltonian are solved immediately if $x_i = 0$. For $x_i \neq 0$ the transformation

$$\begin{bmatrix} \delta x \\ \delta y \end{bmatrix} = \mathbf{T} \begin{bmatrix} \delta X \\ \delta Y \end{bmatrix}, \quad \begin{bmatrix} \delta p_x \\ \delta p_y \end{bmatrix} = \mathbf{T} \begin{bmatrix} \delta P_X \\ \delta P_Y \end{bmatrix}, \quad \text{(A9)}$$

with

$$\mathbf{T} = \begin{bmatrix} \dfrac{\sqrt{x_i^2 + y_i^2 + y_i\sqrt{x_i^2 + y_i^2}}}{\sqrt{2}\sqrt{x_i^2 + y_i^2}} & \dfrac{-x_i}{\sqrt{2}\sqrt{x_i^2 + y_i^2 + y_i\sqrt{x_i^2 + y_i^2}}} \\ \dfrac{x_i\sqrt{x_i^2 + y_i^2 + y_i\sqrt{x_i^2 + y_i^2}}}{\sqrt{2}\sqrt{x_i^2 + y_i^2}(\sqrt{x_i^2 + y_i^2} + y_i)} & \dfrac{\sqrt{x_i^2 + y_i^2} + y_i}{\sqrt{2}\sqrt{x_i^2 + y_i^2 + y_i\sqrt{x_i^2 + y_i^2}}} \end{bmatrix}, \quad \text{(A10)}$$

gives $H_{VH}(\delta x, \delta y, \delta p_x, \delta p_y; t_i)$ the diagonal form

$$H_{VHD}(\delta X, \delta Y, \delta P_x, \delta P_y) = \tfrac{1}{2}(\delta P_x^2 + \delta P_y^2) + \tfrac{1}{2}\{(1 + 2\sqrt{x_i^2 + y_i^2})\delta X^2 + (1 - 2\sqrt{x_i^2 + y_i^2})\delta Y^2\}. \quad \text{(A11)}$$

The columns of matrix $\mathbf{T}$ are the eigenvectors of matrix

$$\mathbf{D}_V^2(\vec{q}(t_i)) \equiv \mathbf{D}_B^2(x_i, y_i) = \begin{bmatrix} 1 + 2y_i & 2x_i \\ 2x_i & 1 - 2y_i \end{bmatrix}, \quad \text{(A12)}$$

and $\lambda_{1,2} = 1 \pm 2\sqrt{x_i^2 + y_i^2}$ are the corresponding eigenvalues.

b. Symplectic integration of the TDH (A3) in an extended phase space. Considering the TDH (A3) as a time-dependent Hamiltonian, we can transform it to a time-independent one having time t as an additional generalized position by the procedure presented in Sec. VI B 2. The 3D Hamiltonian (32) takes the form

$$\tilde{H}_{VH}(\delta x, \delta y, t, \delta p_x, \delta p_y, p_t) = \tfrac{1}{2}(\delta p_x^2 + \delta p_y^2) + p_t + \tfrac{1}{2}\{[1 + 2y(t)]\delta x^2 + [1 - 2y(t)]\delta y^2 + 2[2x(t)]\delta x \delta y\}, \quad \text{(A13)}$$

with p_t being the conjugate momentum of coordinate t. $\tilde{H}_{VH}$ can be split into two integrable parts (33):

$$\tilde{A}(\delta p_x, \delta p_y, p_t) = \tfrac{1}{2}(\delta p_x^2 + \delta p_y^2) + p_t, \quad \tilde{B}(\delta x, \delta y, t) = \tfrac{1}{2}\{[1 + 2y(t)]\delta x^2 + [1 - 2y(t)]\delta y^2 + 2[2x(t)]\delta x \delta y\}, \quad \text{(A14)}$$

so that its equations of motion can be integrated by any symplectic integration method in order to obtain the time evolution of variations δx, δy, δp_x, and δp_y. The maps $e^{\tau L_{\tilde{A}}}$ (34) and $e^{\tau L_{\tilde{B}}}$ (35) (neglecting the equations for p_t) are

$$e^{\tau L_{\tilde{A}}}: \begin{cases} \delta x' = \delta x + \delta p_x \tau \\ \delta y' = \delta y + \delta p_y \tau \\ t' = t + \tau \\ \delta p_x' = \delta p_x \\ \delta p_y' = \delta p_y, \end{cases} \quad \text{(A15)}$$

$$e^{\tau L_{\tilde{B}}}:\begin{cases}\delta x' = \delta x\\ \delta y' = \delta y\\ t' = t\\ \delta p_x' = \delta p_x - \{[1+2y(t)]\delta x + 2x(t)\delta y\}\tau\\ \delta p_y' = \delta p_y + \{-2x(t)\delta x + [-1+2y(t)]\delta y\}\tau.\end{cases} \tag{A16}$$

The corrector term $\tilde{C}$ (36) is

$$\tilde{C} = [\delta x + 2x(t)\delta y + 2y(t)\delta x]^2 + [\delta y + 2x(t)\delta x - 2y(t)\delta y]^2, \tag{A17}$$

and the corresponding map $e^{\tau L_{\tilde{C}}}$ (37) is

$$e^{\tau L_{\tilde{C}}}:\begin{cases}\delta x' = \delta x\\ \delta y' = \delta y\\ t' = t\\ \delta p_x' = \delta p_x - 2(4x(t)\delta y + \{4x^2(t) + [1+2y(t)]^2\}\delta x)\tau\\ \delta p_y' = \delta p_y - 2(4x(t)\delta x + \{4x^2(t) + [1-2y(t)]^2\}\delta y)\tau.\end{cases} \tag{A18}$$

c. Tangent map method. According to the TM method presented in Sec. VI C Eqs. (A1) and (A2) form a set of equations which defines the act of the differential operator L_{HV} on vector $\vec{u}=(x,y,p_x,p_y,\delta x,\delta y,\delta p_x,\delta p_y)$ [Eqs. (41)]. This set of equations is split into two integrable sets

$$\left.\begin{aligned}&\dot{x} = p_x\\ &\dot{y} = p_y\\ &\dot{p}_x = 0\\ &\dot{p}_y = 0\\ &\dot{\delta x} = \delta p_x\\ &\dot{\delta y} = \delta p_y\\ &\dot{\delta p}_x = 0\\ &\dot{\delta p}_y = 0\end{aligned}\right\} \Rightarrow \frac{d\vec{u}}{dt} = L_{AV}\vec{u}, \tag{A19}$$

$$\left.\begin{aligned}&\dot{x} = 0\\ &\dot{y} = 0\\ &\dot{p}_x = -x - 2xy\\ &\dot{p}_y = y^2 - x^2 - y\\ &\dot{\delta x} = 0\\ &\dot{\delta y} = 0\\ &\dot{\delta p}_x = -(1+2y)\delta x - 2x\delta y\\ &\dot{\delta p}_y = -2x\delta x + (-1+2y)\delta y\end{aligned}\right\} \Rightarrow \frac{d\vec{u}}{dt} = L_{BV}\vec{u}, \tag{A20}$$

which define the act of operators L_{AV} (44) and L_{BV} (45), respectively. Then, maps $e^{\tau L_{AV}}$ (46) and $e^{\tau L_{AV}}$ (47) are

$$e^{\tau L_{AV}}:\begin{cases}x' = x + p_x\tau\\ y' = y + p_y\tau\\ p_{x'} = p_x\\ p_{y'} = p_y\\ \delta x' = \delta x + \delta p_x\tau\\ \delta y' = \delta y + \delta p_y\tau\\ \delta p_x' = \delta p_x\\ \delta p_y' = \delta p_y,\end{cases} \tag{A21}$$

$$e^{\tau L_{BV}}:\begin{cases}x' = x\\ y' = y\\ p_x' = p_x - x(1+2y)\tau\\ p_y' = p_y + (y^2 - x^2 - y)\tau\\ \delta x' = \delta x\\ \delta y' = \delta y\\ \delta p_x' = \delta p_x - [(1+2y)\delta x + 2x\delta y]\tau\\ \delta p_y' = \delta p_y + [-2x\delta x + (-1+2y)\delta y]\tau,\end{cases} \tag{A22}$$

while the map $e^{\tau L_{CV}}$ (53) of the corrector function C (A7) is

$$e^{\tau L_{CV}}:\begin{cases}x' = x\\ y' = y\\ p_x' = p_x - 2x(1+2x^2+6y+2y^2)\tau\\ p_y' = p_y - 2(y-3y^2+2y^3+3x^2+2x^2y)\tau\\ \delta x' = \delta x\\ \delta y' = \delta y\\ \delta p_x' = \delta p_x - 2[(1+6x^2+2y^2+6y)\delta x + 2x(3+2y)\delta y]\tau\\ \delta p_y' = \delta p_y - 2[2x(3+2y)\delta x + (1+2x^2+6y^2-6y)\delta y]\tau.\end{cases} \tag{A23}$$

[1] E. Hairer, S. P. Nørsett, and G. Wanner, *Solving Ordinary Differential Equations: Nonstiff Problems*, Springer Series in Computational Mathematics Vol. 8, 2nd ed. (Springer, New York, 1993).

[2] E. Hairer, C. Lubich, and G. Wanner, *Geometric Numerical Integration: Structure-Preserving Algorithms for Ordinary Differential Equations*, Springer Series in Computational Mathematics Vol. 31 (Springer, New York, 2002).

[3] R. I. McLachlan and G. R. W. Quispel, J. Phys. A **39**, 5251 (2006); É. Forest, *ibid.* **39**, 5321 (2006).

[4] Ch. Skokos, Lect. Notes Phys. **790**, 63 (2010).

[5] J. Laskar, Physica D **67**, 257 (1993); *Hamiltonian Systems with Three or More Degrees of Freedom*, edited by C. Simó (Kluwer Academic Publishers, Dordrecht, 1999), p. 134.

[6] C. Froeschlé, E. Lega, and R. Gonczi, Celest. Mech. Dyn. Astron. **67**, 41 (1997); C. Froeschlé, R. Gonczi, and E. Lega, Planet. Space Sci. **45**, 881 (1997).

[7] R. Barrio, Chaos, Solitons Fractals **25**, 711 (2005); Int. J. Bifurcation Chaos **16**, 2777 (2006).

[8] Ch. Skokos, J. Phys. A **34**, 10029 (2001); Ch. Skokos, Ch. Antonopoulos, T. C. Bountis, and M. N. Vrahatis, Prog. Theor. Phys. Suppl. **150**, 439 (2003); J. Phys. A **37**, 6269 (2004).

[9] Ch. Skokos, T. C. Bountis, and Ch. Antonopoulos, Physica D **231**, 30 (2007).

[10] Ch. Skokos, T. C. Bountis, and Ch. Antonopoulos, Eur. Phys. J. Spec. Top. **165**, 5 (2008).

[11] P. M. Cincotta and C. Simó, Astron. Astrophys. Suppl. Ser. **147**, 205 (2000); P. M. Cincotta, C. M. Giordano, and C. Simó, Physica D **182**, 151 (2003).

[12] A. M. Lyapunov, *The General Problem of the Stability of Motion* (Taylor & Francis, London, 1992); English translation from French: A. Liapounoff, Ann. Fac. Sci. Toulouse Math. **9**, 203 (1907); the French text was reprinted in *Annals of Mathematics Studies* (Princeton University Press, Princeton, NJ, 1947), Vol. 17, and the original was published in Russian by the Mathematical Society of Kharkov in 1892.

[13] V. I. Oseledec, Trans. Mosc. Math. Soc. **19**, 197 (1968).

[14] G. Benettin, L. Galgani, and J.-M. Strelcyn, Phys. Rev. A **14**, 2338 (1976).

[15] Y. B. Pesin, Russ. Math. Surveys **32**, 55 (1977).

[16] G. Benettin, L. Galgani, A. Giorgilli, and J.-M. Strelcyn, Meccanica **15**, 9 (1980).

[17] G. Benettin, L. Galgani, A. Giorgilli, and J.-M. Strelcyn, Meccanica **15**, 21 (1980).

[18] G. Benettin, L. Galgani, A. Giorgilli, and J.-M. Strelcyn, C.R. Seances Acad. Sci., Ser. A **286**, 431 (1978).

[19] W. H. Press, S. A. Teukolsky, W. T. Vetterling, and B. P. Flannery, *Numerical Recipes in FORTRAN: The Art of Scientific Computing*, 2nd ed. (Cambridge University Press, Cambridge, England, 1992).

[20] T. Manos, Ch. Skokos, and T. Bountis, in *Proceedings of the CCT 07*, edited by C. Chandre, X. Leoncini, and G. Zaslavsky (World Scientific, Singapore, 2008), p. 356; D. D. Carpintero, Mon. Not. R. Astron. Soc. **388**, 1293 (2008); T. Manos, Ch. Skokos, and T. Bountis, in *Astrophysics and Space Science Proceedings*, edited by G. Contopoulos and P. A. Patsis (Springer-Verlag, Berlin, 2009), p. 367; T. Bountis, T. Manos, and H. Christodoulidi, J. Comput. Appl. Math. **227**, 17 (2009); Ch. Antonopoulos, V. Basios, and T. Bountis, Phys. Rev. E **81**, 016211 (2010).

[21] J. Laskar and P. Robutel, Celest. Mech. Dyn. Astron. **80**, 39 (2001).

[22] Note that in [21] the Poisson bracket (19) is defined with opposite signs.

[23] P. J. Channell and C. Scovel, Nonlinearity **3**, 231 (1990); É. Forest and R. D. Ruth, Physica D **43**, 105 (1990); H. Yoshida, Phys. Lett. A **150**, 262 (1990); J. Candy and W. Rozmus, J. Comput. Phys. **92**, 230 (1991); R. I. McLachlan and P. Atela, Nonlinearity **5**, 541 (1992); H. Yoshida, Celest. Mech. Dyn. Astron. **56**, 27 (1993); I. P. Omelyan, I. M. Mryglod, and R. Folk, Phys. Rev. E **65**, 056706 (2002).

[24] R. I. McLachlan, BIT **35**, 258 (1995).

[25] In [21] this commutator is denoted as $C=\{\{A,B\},B\}$ due to the different definition of the Poisson bracket (19) used.

[26] L. Nadolski, Ph.D. thesis, University of Paris XI, 2001; L. Nadolski and J. Laskar, Proceedings of the European Particle Accelerator Conference 2002 (EPAC02) (unpublished), p. 1276; Ch. Skokos and Y. Papaphilippou, Proceedings of the European Particle Accelerator Conference 2008 (EPAC08) (unpublished), p. 682.

[27] S. Flach, D. O. Krimer, and Ch. Skokos, Phys. Rev. Lett. **102**, 024101 (2009); Ch. Skokos, D. O. Krimer, S. Komineas, and S. Flach, Phys. Rev. E **79**, 056211 (2009); Ch. Skokos and S. Flach, *ibid.* **82**, 016208 (2010); T. V. Laptyeva, J. D. Bodyfelt, D. O. Krimer, Ch. Skokos, and S. Flach, EPL **91**, 30001 (2010).

[28] S. A. Chin, Phys. Lett. A **226**, 344 (1997).

[29] I. P. Omelyan, I. M. Mryglod, and R. Folk, Phys. Rev. E **66**, 026701 (2002); Comput. Phys. Commun. **151**, 272 (2003).

[30] Freely available at http://www.unige.ch/~hairer/software.html

[31] A. J. Lichtenberg and M. A. Lieberman, *Regular and Chaotic Dynamics*, 2nd ed. (Springer, Berlin, 1992).

[32] M. Hénon and C. Heiles, Astron. J. **69**, 73 (1964).

[33] G. Contopoulos, L. Galgani, and A. Giorgilli, Phys. Rev. A **18**, 1183 (1978).

[34] E. Fermi, J. Pasta, and S. Ulam, Los Alamos National Laboratory Report No. LA-1940, 1955 (unpublished); G. P. Berman and F. M. Izrailev, Chaos **15**, 015104 (2005).

[35] S. Paleari and T. Penati, Lect. Notes Phys. **728**, 239 (2008).

[36] V. Latora, A. Rapisarda, and S. Ruffo, Phys. Rev. Lett. **80**, 692 (1998); A.-S. Libert, C. Hubaux, and T. Carletti, e-print arXiv:1005.5611.

[37] S. Mikkola and K. Innanen, Celest. Mech. Dyn. Astron. **74**, 59 (1999); M. Guzzo, Icarus **174**, 273 (2005).

[38] S. K. Gray, D. W. Noid, and B. G. Sumpter, J. Chem. Phys. **101**, 4062 (1994).

[39] G. Tancredi, A. Sánchez, and F. Roig, Astron. J. **121**, 1171 (2001); X. Wu and T.-Y. Huang, Phys. Lett. A **313**, 77 (2003); X. Wu, T.-Y. Huang, and H. Zhang, Phys. Rev. D **74**, 083001 (2006).